

Paleoceanography and Paleoclimatology



RESEARCH ARTICLE

10.1029/2022PA004533

Key Points:

- Source signal of TEX_{86} proxy is likely derived from depths shallower than 350 m at Chilean and Angola margins
- OH-GDGT based proxies show similar variability as TEX_{86} records, but show regional differences in their absolute temperature estimates
- $\text{U}_{37}^{\text{K}'}$ proxy signal may be impacted by post-depositional changes or lateral transport even for closely located cores

Supporting Information:

Supporting Information may be found in the online version of this article.

Correspondence to:






D. Varma,
devika.varma@nioz.nl

Citation:

Varma, D., Hättig, K., van der Meer, M. T. J., Reichart, G.-J., & Schouten, S. (2023). Constraining water depth influence on organic paleotemperature proxies using sedimentary archives. *Paleoceanography and Paleoclimatology*, 38, e2022PA004533. <https://doi.org/10.1029/2022PA004533>

Received 24 AUG 2022
Accepted 22 MAY 2023

Constraining Water Depth Influence on Organic Paleotemperature Proxies Using Sedimentary Archives

Devika Varma¹ , Katrin Hättig¹ , Marcel T. J. van der Meer¹ , Gert-Jan Reichart^{2,3} , and Stefan Schouten^{1,2} 

¹Department of Marine Microbiology and Biogeochemistry, NIOZ Royal Netherlands Institute for Sea Research, Texel, The Netherlands, ²Department of Earth Sciences, Faculty of Geosciences, Utrecht University, Utrecht, The Netherlands, ³Department of Ocean Systems, NIOZ Royal Netherlands Institute for Sea Research, Texel, The Netherlands

Abstract The TEX_{86} paleothermometer has been extensively used to reconstruct past sea water temperatures, but it remains unclear which export depths the proxy represents. Here we used a novel approach to better constrain the proxy recording depths by investigating paleotemperature proxies (TEX_{86} , $\text{U}_{37}^{\text{K}'}$, RI–OH and RI–OH') from two pairs of proximal (<12 km apart) cores from Chilean and Angola margins, respectively. These cores are from steep continental slopes and lower shelves, which leads to a substantial difference in water depth between them despite being closely located. Surprisingly, the deep and the shallow $\text{U}_{37}^{\text{K}'}$ records at the Chilean margin show dissimilarities, in contrast to the similar records from the Angola margin, which may be due to post-depositional alteration at the former sites. In contrast, the TEX_{86} records were statistically indistinguishable between the sites at both the locations, even though the GDGT [2]/[3] ratio suggests GDGTs derived from potentially different archaeal communities residing at different depths. A short-lived difference between the TEX_{86} records is observed during the last glacial period at the Angola margin, possibly due to a contribution of Antarctic Intermediate Waters to the deep site. Modelling suggests that the TEX_{86} source signal at our core sites reaches its peak abundance at water depths shallower than 350 m. The RI–OH and RI–OH' records show similar variability as the TEX_{86} records, although regional differences in their absolute temperature estimates exist. Our approach using proximal sediment cores at steep slopes appears useful to constrain the export depth of organic proxy signals for paleo-reconstructions.

1. Introduction

The TEX_{86} (TetraEther index of 86 carbons; Schouten et al., 2002), based on glycerol dialkyl glycerol tetraethers (GDGTs), has proven invaluable especially with regard to reconstructing sea water temperatures from deep geologic history (e.g., Jenkyns et al., 2004, 2012; Sluijs et al., 2006, 2020; Steinig et al., 2020) where other paleothermometers (like $\text{U}_{37}^{\text{K}'}$, Mg/Ca, Long-chain Diol Index) become unreliable or proxy carriers are not detected (e.g., Bentaleb et al., 2002; de Bar et al., 2019; Pelejero & Grimalt, 1997; Regenberg et al., 2014). The TEX_{86} proxy, however has limitations, for example, due to seasonal and depth changes of the source signal, multiple source organisms for these GDGT lipids and their different community structure (e.g., Huguet et al., 2007; Jia et al., 2012; Lopes Dos Santos et al., 2013; Pitcher, Wuchter, et al., 2011; Weijers et al., 2006). The availability of nutrients and oxygen during growth of these organisms could also affect the TEX_{86} proxy (Elling et al., 2014; Hurley et al., 2016; Qin et al., 2015). One of the main topics of debate is the depth of the marine source signal of TEX_{86} , in order to use it as a sea surface temperature (SST) or a sub-surface temperature, or even a bottom water temperature proxy at different locations (e.g., Hines et al., 2017; Huguet et al., 2007; Hurley et al., 2018; Jia et al., 2012; Kim et al., 2015; Tierney & Tingley, 2015). This problem derives from the fact that Thaumarchaeota, thought to be the main source of GDGTs in the marine environment (e.g., Besseling et al., 2020; Pitcher, Villanueva, et al., 2011; Schouten et al., 2008; Zeng et al., 2019), are known to thrive throughout the water column (e.g., Herndl et al., 2005; Karner et al., 2001; Wuchter et al., 2005).

Studies based on 16S rRNA and *amoA* genes suggest that the Thaumarchaeota often maximize in their abundance in shallow sub-surface waters (e.g., Church et al., 2010; Francis et al., 2005; Hu et al., 2011; Massana et al., 1997; Schouten et al., 2012; Sollai et al., 2019). It is speculated that GDGT export mainly occurs through sinking fecal pellets of grazing organisms which are mainly derived from the upper water column (Wakeham et al., 2003; Wuchter et al., 2005), therefore leading to a predominantly (sub) surface signal. Suspended particulate matter (SPM) studies from ocean water columns also indicate the highest concentration of crenarchaeol, the

© 2023. The Authors.

This is an open access article under the terms of the [Creative Commons Attribution License](https://creativecommons.org/licenses/by/4.0/), which permits use, distribution and reproduction in any medium, provided the original work is properly cited.

biomarker for Thaumarchaeota (Sinninghe Damsté, Schouten, et al., 2002), at sub-surface waters (e.g., Hurley et al., 2016, 2018; Schouten et al., 2012; Sollai et al., 2015). A core-top study of compiled TEX_{86} data from the tropical to sub-tropical regions in both the Pacific and the Atlantic Ocean suggests a surface to shallow sub-surface origin of its source signal (Zhang & Liu, 2018). In contrast, radiocarbon measured on GDGTs from the Santa Monica basin indicates a contribution of sedimentary GDGTs from deep-water dwelling archaea from >200 m depths (Pearson et al., 2001; Shah et al., 2008). Studies from other locations have also suggested export of GDGTs from the mesopelagic zone (Kim et al., 2015; Taylor et al., 2013), leading to the idea that deeper signals from the mesopelagic zone are important (cf. Ho & Laepple, 2016).

Molecular ecological analyses have shown that different Thaumarchaeotal populations reside at different water depths (e.g., Besseling et al., 2019; Sollai et al., 2019; Techtman et al., 2017; Villanueva et al., 2015), and several studies have shown that in certain regions the deep water communities contribute a substantial amount of GDGTs to the underlying sediments (Kim et al., 2015; Park et al., 2019). A way to diagnose the contributions of different archaeal communities is through the GDGT [2]/[3] ratio, which varies between archaeal communities, leading to generally increasing GDGT [2]/[3] ratios with increasing water depth (Taylor et al., 2013; Villanueva et al., 2015). A recent study by Rattanasriampaipong et al. (2022) has revealed distinct GDGT [2]/[3] signatures and thermal distribution patterns of GDGTs in different archaeal ecotypes. The direct impact of this changing GDGT [2]/[3] ratio on the TEX_{86} is in itself limited, as both GDGTs appear in the numerator as well as the denominator of the TEX_{86} definition.

In addition to isoprenoid GDGTs used in TEX_{86} , another class of lipids, the hydroxy-GDGTs (OH-GDGTs) used in RI–OH and RI–OH' SST proxies, has received recent interest, particularly for polar regions (Fietz et al., 2020; Lü et al., 2015). OH-GDGTs are also known to be produced by Thaumarchaeota, as well as some Euryarchaeota (Bale et al., 2019; Elling et al., 2015; Lipp & Hinrichs, 2009; Liu, Lipp, et al., 2012; Liu, Summons, & Hinrichs, 2012; Schouten et al., 2008; Summons et al., 2002). Liu, Lipp, et al. (2012) and Liu, Summons, & Hinrichs (2012) have ascribed the difference in ring distribution between non-hydroxylated iGDGTs and OH-GDGTs to separate source organisms or production under different environmental stressors. However, the high correlation between OH-GDGT-0 and crenarchaeol concentrations, the latter being specific to Thaumarchaeota, from water column samples and surface sediments suggests a common source in the marine environment (Fietz et al., 2013). Initial applications of these proxies showed promising results where they seem to systematically capture temperature variability from the past, consistent with other proxies (e.g., Allaart et al., 2020; Davtian et al., 2019, 2021; Kremer et al., 2018). Still, differences were observed between OH-GDGT reconstructed absolute temperatures and those based on TEX_{86} and $U_{37}^{K'}$ (Davtian et al., 2019; Vorrath et al., 2020), which may indicate differences in the depths these proxies reflect.

Here we investigate the potential impact of water depth on the organic temperature proxies TEX_{86} , RI–OH and RI–OH' by analyzing a pair of cores from the Chilean margin and a pair of cores from the Angola margin covering the last ~40–50 Kyr. From both locations, the cores are retrieved from sites close to each other (<12 km apart) and, hence, they are likely receiving the same surface signal, but since they are located at strongly different water depths (1,015 m vs. 489 m and 738 vs. 426 m for the Chilean and the Angola margin cores, respectively), they accumulate different extents of sub-surface material. By comparing the TEX_{86} records of the two areas as well as comparing them with the $U_{37}^{K'}$ based records, known to reflect surface temperatures, we attempt to constrain export depth of the source signal for the GDGT based temperature proxies. Additionally, we try to constrain depths represented by GDGT based temperature proxies by modelling different depth distributions of GDGTs in the water column based on the modern-day ocean.

2. Materials and Methods

2.1. Study Area and Sites

2.1.1. Chilean Margin

ODP 202 Sites 1234 (36.22°S, 73.68°W) and 1235 (36.16°S, 73.57°W) are proximally located and ~12 km apart from each other in the southeast Pacific Ocean (Mix et al., 2003) (Figure 1a). The sites are located at water depths of 1,015 m and 489 m and from here on are referred to as the deep site and the shallow site from the Chilean margin, respectively. The present-day annual mean SST in the study area is 13°C with a seasonal amplitude of 1.4°C (Locarnini et al., 2019). The location is near to the river mouths of the Río Bio-Bio and Río Itata river

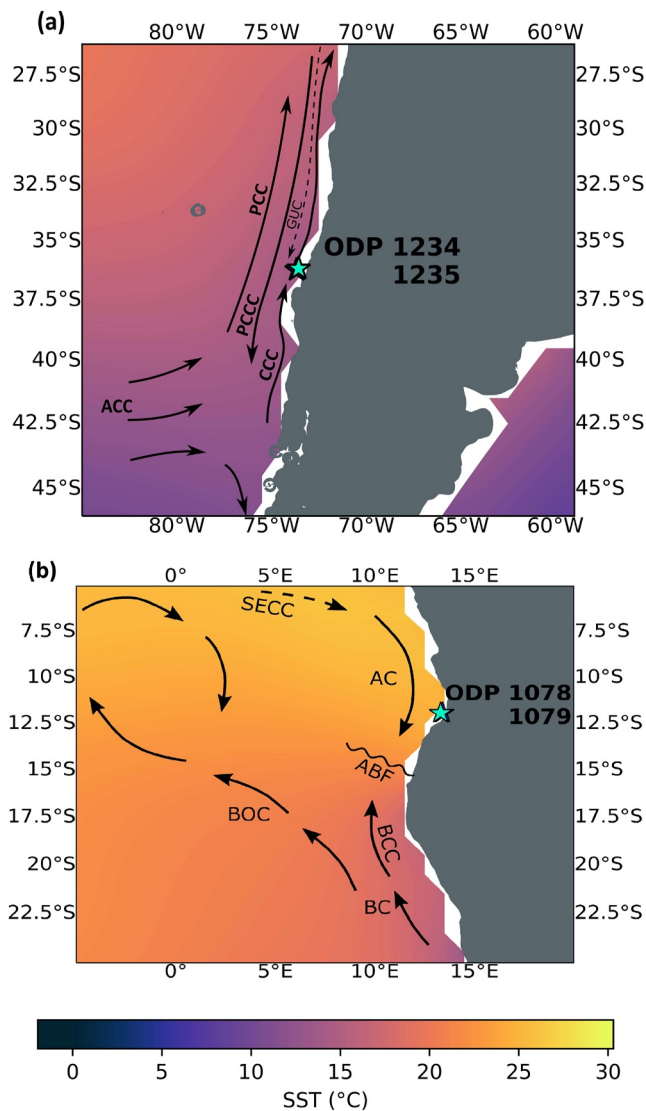


Figure 1. Map of study sites and modern sea surface temperature (Locarnini et al., 2019) at the (a) Chilean margin Sites 1234 and 1235; ACC = Antarctic Circumpolar Current; CCC = Chile Coastal Current; PCC = Peru-Chile Current; PCCC = Peru-Chile Countercurrent; GUC = Gunther Undercurrent; (b) Angola margin- Sites 1078 and 1079; AC = Angola Current; BC = Benguela Current; ABF = Angola-Benguela Front; BCC = Benguela Coastal Current; BOC = Benguela Ocean Current; SECC = South Equatorial Countercurrent. Stars indicate the location of the sites. Undercurrents are in dashed lines and surface currents are in solid lines.

systems and hence could be influenced by fluvial inputs (Muratli, Chase, McManus, & Mix, 2010).

The area is under the influence of the Humboldt Current system, which is here mainly expressed by an equatorward flowing northern branch of the bifurcating nutrient rich Antarctic Circumpolar Current (ACC), known as Peru-Chile Current (PCC) or Humboldt Current (Hebbeln et al., 2000; Strub et al., 1998). Close to the coast, the Chile Coastal Current (CCC), which flows predominantly equatorward, shows a seasonal reversal at our study site where it flows poleward during winter (Thiel et al., 2007). Between the PCC and the coastal current, the Peru-Chile Countercurrent (PCCC) flows poleward. At the coastal margin, underlying the nutrient rich PCC is a poleward flowing Gunther (or Peru-Chile) Undercurrent (GUC), located between 100–300 m water depths. The water of the GUC consists of nutrient rich, oxygen-poor, highly saline water, and is the source of the upwelled water close to the coast, where our sites are located (Morales et al., 1996). Underlying the GUC, from around 300–1,200 m water depth is the equatorward flowing low salinity, oxygen rich Antarctic Intermediate Water (AAIW) (Hebbeln et al., 2000; Strub et al., 1998). At present day, the coring-site 1235 is located at a water depth in the transition zone between GUC and AAIW (Tiedemann et al., 2007). Below ~1,200 m the oxygen poor, sluggish water mass of Pacific Deep Water (PDW) flows poleward (Hebbeln et al., 2000).

The 1234 and 1235 sediment cores were sampled with a resolution of one sample per ~2 Kyr (thousand years) and 1 Kyr, respectively, for the last 40 Kyr. A total of 41 samples from Site 1235 and 20 samples from Site 1234 were used in this study. The age-depth models of Site 1234 and 1235 for the last 40 Kyr are based on radiocarbon ages measured on mixed benthic foraminifera (Muratli, Chase, Mix, & McManus, 2010). Additionally, three radiocarbon measurements were obtained with the Mini-Carbon-Dating-System (MICADAS) at the Alfred-Wegener-Institute (AWI). With the high precision compact accelerator mass spectrometer, gas analyses of small sized samples of the benthic foraminifera species *Uvigerina* from Site 1235 were performed. The last tie-point for both cores marks the Laschamp event at 41,000 years before present (BP), based on correlating magnetic susceptibility between ODP cores 1233, 1234 and 1235 (Mix et al., 2003). Since the tie points at 41 Kyr with 27 and 51 m composite depth, for Sites 1234 and 1235, respectively, are rough estimations (Mix et al., 2003), the data points in the record between 30 and 40 Kyr ago likely have an uncertainty of around ± 1 Kyr although the sedimentation rate is assumed to be constant. Radiocarbon ages were converted to calendar years using Marine09 data set (Reimer et al., 2009) with the reservoir age correction given by Muratli, Chase, Mix & McManus (2010). The core chronology was constructed with the statistical package Bacon (Blaauw & Christeny, 2011) using a Bayesian approach.

2.1.2. Angola Margin

Similar to the Chilean margin, two closely located sediment cores (~10 km apart) from the Angola margin were used in this study. ODP 175 Site 1078 (11.92°S, 13.40°E) and 1079 (11.93°S, 13.31°E) are from water depths of 426 and 738 m (Mix et al., 2003) and here on referred to as the shallow site and the deep site from the Angola margin, respectively (Figure 1b). The modern seasonal temperature range at this location is 20.9–28.2°C with an annual mean SST of 24.8°C (Locarnini et al., 2019).

The main surface current in our study area is the oxygen- and nutrient-poor poleward flowing Angola Current (AC), which brings in warm tropical South Atlantic Central Water (SACW) to the continental shelf and slope of Angola from surface to water depths of 250–300 m (Moroshkin et al., 1970; Poole & Tomczak, 1999). The AC is

mainly fed by the South Equatorial Countercurrent (SECC) and meets the cold, nutrient-rich, northward flowing Benguela Current (BC) at $\sim 16^{\circ}\text{S}$, forming the Angola-Benguela Front (ABF). North of the ABF, where our two sites are located, is under the influence of the West African monsoon where hardly any coastal upwelling occurs (Shannon et al., 1987). Though seasonal oceanic upwelling as a part of the Angola Dome circulation influences primary productivity in this region. Our study area is not influenced by riverine input from the Congo plume (Wefer et al., 1998), though fluvial transport from the Balombo River is likely to occur (Dupont et al., 2008). South of the ABF, south-east trade winds cause coastal upwelling. The temperature gradient across the ABF becomes more pronounced when strong trade winds are present and causes enhanced upwelling in the south of the ABF and strong intrusion of warm tropical waters by the Angola current north of the ABF (Kim et al., 2003). In the Angola basin $\sim 11^{\circ}\text{S}$, the central water layer below the AC is solely composed of SACW, which remains stable on seasonal time-scales (Kopte et al., 2017; Mohrholz et al., 2008). Underlying the SACW is the AAIW at depths of $\sim 500\text{--}800$ m, transitioning into North Atlantic Deep Water (NADW) below $\sim 1,500$ m (Shannon & Nelson, 1996; Siegfried et al., 2019).

The average sampling resolution for both the Sites 1078 and 1079 is about one sample per 2.5 Kyr. We analysed a total of 28 samples from Site 1078 and 27 samples from Site 1079. The age model for Site 1078 Hole C is based on ^{14}C dating of planktonic foraminiferal tests and mollusks as reported by Kim et al. (2003) and Rühlemann et al. (2004) for 0–22 Kyr, and after Dupont et al. (2008) for 25–42 Kyr. For ages between ~ 22 and 25 Kyr ago, a linear interpolation was used and for 42–50 Kyr, the age-depth model was extrapolated by assuming a constant sedimentation rate based on the last two calibrated ages from Dupont et al. (2008). For Site 1079 Hole A, the age-depth model is based on cross-correlating $\delta^{18}\text{O}$ values of *Globobulimina* spp. and age control points after Pérez et al. (2001). Since the age model was publicly unavailable, a digitizing tool- WebPlotDigitizer, version 4 (<https://automeris.io/WebPlotDigitizer>) was used to retrieve the $\delta^{18}\text{O}$ data and sedimentation rates from a published figure in Pérez et al. (2001).

2.2. Lipid Extraction and Analysis

Samples from ODP Sites 1235, 1078 and 1079 were extracted and analyzed as described below, while samples from sediment core 1234 were previously extracted and analyzed by de Bar et al. (2018).

All samples were freeze-dried and homogenized with mortar and pestle. Lipids were extracted using accelerated solvent extractor (ASE 200, DIONEX) at 100°C and $7\text{--}8 \times 10^6$ Pa pressure with a dichloromethane (DCM): methanol (MeOH) (9:1, v/v) mixture. Extracts were dried under a N_2 gas flow using a Caliper TurboVap LV and passed over a Na_2SO_4 column, after re-dissolving it in DCM:MeOH (9:1, v/v) to remove remaining water. After drying under N_2 and weighing, ~ 3 mg of the total lipid extract (TLE) was desulphurized with copper turnings activated with 2 N HCl overnight and passed over a Na_2SO_4 column again using DCM:MeOH (9:1, v/v). The extracts were dried down under N_2 and separated into apolar, ketone and polar fractions using an activated Al_2O_3 column with hexane:DCM (9:1, v/v), hexane:DCM (1:1, v/v) and DCM:MeOH (1:1, v/v) mixtures, respectively.

The ketone fractions, containing the alkenones, were dissolved in ethyl acetate and analyzed for alkenones using an Agilent 6890N gas chromatograph with flame ionization detection (GC-FID) equipped with a CP Sil-5 fused silica capillary column ($50\text{ m} \times 0.32\text{ mm}$, $0.12\text{ }\mu\text{m}$ thickness). Helium was used as the carrier gas. The GC temperature condition was 70°C initially and increased to 200°C at the rate of $20^{\circ}\text{C min}^{-1}$, and then increased to 320°C at $3^{\circ}\text{C min}^{-1}$ and held there for 45 min. The $U_{37}^{K'}$ values were calculated according to Prahl and Wakeham (1987) (Equation 1) from the abundance of di- and tri-unsaturated C_{37} alkenones. The global core-top calibration of Müller et al. (1998) (Equation 2) was used to calculate $U_{37}^{K'}$ -based SSTs.

$$U_{37}^{K'} = \frac{[\text{C}_{37:2}]}{[\text{C}_{37:2}] + [\text{C}_{37:3}]} \quad (1)$$

$$\text{SST} = \frac{U_{37}^{K'} - 0.044}{0.033} \quad (2)$$

The polar fractions, containing the GDGTs and OH-GDGTs, were dried under N_2 and dissolved in hexane:isopropanol (99:1, v/v) and filtered through $0.45\text{ }\mu\text{m}$ PTFE filter. The filtered polar fractions were analyzed for isoprenoid-, branched- and OH-GDGTs by ultra-high performance liquid chromatography/mass spectrometry (UHPLC/MS) on an Agilent 1260 Infinity HPLC coupled to Agilent 6130 MSD. GDGT sepa-

ration was done in normal phase according to Hopmans et al. (2016) using two silica BEH HILIC columns (2.1 mm × 150 mm, 1.7 μm thickness) connected in series and maintained at 25°C. A solvent gradient of hexane:isopropanol (9:1, v/v) (solvent A) and hexane (solvent B) was used starting with 18% of A and 82% of B at a constant flow rate of 0.2 ml min⁻¹ eluted isocratically for 25 min and thereafter increasing A in a linear gradient to 30% in 25 min and to 100% A in the following 30 min. GDGTs were detected in Selective Ion Monitoring (SIM) mode for protonated GDGT molecules [M+H]⁺. The TEX₈₆ index was calculated according to Schouten et al. (2002) and TEX₈₆^H according to Kim et al. (2010) (Equations 3 and 4). BAYSPAR SST with the default parameters in the Standard Prediction method was used to estimate temperatures after Tierney and Tingley (2014, 2015).

$$\text{TEX}_{86} = \frac{[\text{iGDGT} - 2] + [\text{iGDGT} - 3] + [\text{Cren}']}{[\text{iGDGT} - 1] + [\text{iGDGT} - 2] + [\text{iGDGT} - 3] + [\text{Cren}']} \quad (3)$$

$$\text{TEX}_{86}^{\text{H}} = \log(\text{TEX}_{86}) \quad (4)$$

The RI–OH and RI–OH' temperature proxies based on OH-GDGTs were calculated according to Equations 5 and 6, respectively (Lü et al., 2015). The numbers in Equations 3, 5 and 6 correspond to the number of cyclopentane moieties in the isoprenoid GDGTs (iGDGTs) and OH-GDGTs, respectively. We used the global calibration of Lü et al. (2015) (Equation 7) for RI–OH temperature estimates and the global calibration of Fietz et al. (2020) (Equation 8) for RI–OH' for obtaining SST estimates.

$$\text{RI} - \text{OH} = \frac{[\text{OH} - \text{GDGT} - 1] + 2 \times [\text{OH} - \text{GDGT} - 2]}{[\text{OH} - \text{GDGT} - 1] + [\text{OH} - \text{GDGT} - 2]} \quad (5)$$

$$\text{RI} - \text{OH}' = \frac{[\text{OH} - \text{GDGT} - 1] + 2 \times [\text{OH} - \text{GDGT} - 2]}{[\text{OH} - \text{GDGT} - 0] + [\text{OH} - \text{GDGT} - 1] + [\text{OH} - \text{GDGT} - 2]} \quad (6)$$

$$\text{SST} = \frac{\text{RI} - \text{OH} - 1.11}{0.018} \quad (7)$$

$$\text{SST} = \frac{\text{RI} - \text{OH}' + 0.029}{0.0422} \quad (8)$$

For ODP Site 1234, previously analyzed by de Bar et al. (2018), we reintegrated the chromatograms for alkenones and GDGTs here, to avoid any discrepancies in data handling between individuals. Additionally, OH-GDGT-based proxies, not reported by de Bar et al. (2018), are also evaluated here using these analyses.

Five samples from ODP 1234 and six samples from ODP 1235 showed an unknown compound co-eluting with GDGT-2 and hence TEX₈₆ data of these samples were excluded from any subsequent analysis and not reported here. The Branched and Isoprenoid Tetraether index (BIT) from branched GDGTs was calculated according to Equation 9 (De Jonge et al., 2015; Hopmans et al., 2004).

$$\text{BIT} = \frac{[\text{brGDGT} - \text{Ia}] + [\text{brGDGT} - \text{IIa}] + [\text{brGDGT} - \text{IIa}'] + [\text{brGDGT} - \text{IIIa}] + [\text{brGDGT} - \text{IIIa}']}{[\text{brGDGT} - \text{Ia}] + [\text{brGDGT} - \text{IIa}] + [\text{brGDGT} - \text{IIa}'] + [\text{brGDGT} - \text{IIIa}] + [\text{brGDGT} - \text{IIIa}'] + [\text{Cren}]} \quad (9)$$

Analytical uncertainty was calculated using an in-house standard from a Drammensfjord sediment extract for TEX₈₆ (1σ = 0.015), RI – OH (1σ = 0.01) and RI – OH' (1σ = 0.011) for 31 replicates. For U₃₇^{K'}, four replicates of a sample from ODP core 1079 were used to obtain a 1σ analytical uncertainty of 0.026.

2.3. Statistical Analysis

Direct comparison of different proxy indices between the deep and the shallow sites would involve large uncertainties arising from errors in the age models and the extrapolation needed. Hence, cross correlation of each proxy between the two sites was achieved by binning the data into 2000-year bins. We use bins of 2000 years in accordance with the resolution of our data set. Although this results in one data point per bin for some time periods, especially for Site 1234, using larger bins would not be ideal since it would average out the temperature variability observed in these records. The binned TEX₈₆ record generated this way still reflects the original data set. All the statistical *t*-tests mentioned here were performed on this binned data set. The York regression, which

takes into account the bivariate uncertainties (Mahon, 2010; York et al., 2004), was also used to compare proxy records between the deep and the shallow sites.

2.4. Modelling TEX_{86} Source Signal at Core Sites

To infer the depth the TEX_{86} proxy is derived from, we modelled the depth distributions of GDGTs in the water column at each core location. We also assume that the growth temperature is the only factor controlling the lipid composition in the archaeal cells based on homeoviscous adaptation. Though Thaumarchaeota thrive throughout the water column, their maximum cell numbers and also GDGT abundance occurs at the sub-surface (e.g., Basse et al., 2014; Church et al., 2010; Hurley et al., 2018; Karner et al., 2001; Schouten et al., 2012). We modelled this GDGT abundance pattern by various gamma probability density functions with maximal abundances set at different depths (50–400 m with steps of 50 m) (see Figure S1, Table S1 in Supporting Information S1) to represent possible depth profiles of GDGT abundance in the water column (e.g., Tierney & Tingley, 2015). Although we know that sedimentary export may be more efficient in the upper part of the water column due to mineral ballasting and fecal pellet packaging (Wakeham et al., 2003; Wuchter et al., 2005), it is difficult to constrain this and incorporate it into the model without regional sediment trap studies. We assume here, for the sake of simplicity, that there is an equally efficient export of GDGTs at all depths, though we realize that this is unlikely to be so. Therefore, the GDGT abundance profile in the water column is considered to reflect the respective contribution of each depth to the sedimentary TEX_{86} signal. The $P(d < X < d')$ in Equation 10 denotes the cumulative distribution function (CDF) of the gamma distribution from depths of d to d' meters, normalized to the total probability from surface to the water depth of each site (dashed lines in Figure S1 in Supporting Information S1).

We then obtained depth-weighted temperature signals from modern ocean temperatures (Locarnini et al., 2019) and calculated the modelled temperature (T_{model}) according to Equation 10. We also assume constant and continued settling of particles to the sediment floor throughout the year.

$$T_{\text{model}} = \sum_d \left[P(d < X < d') \times \left(\frac{T_d + T_{d'}}{2} \right) \right] \quad (10)$$

The annual mean temperature at a depth of d meter is denoted by T_d . The d and d' are successive depth intervals using the depth resolution from World Ocean Atlas 2018 temperature data (Locarnini et al., 2019).

We then converted the T_{model} (the temperature the GDGT distribution at each location should reflect) into TEX_{86} values using existing TEX_{86} -temperature calibrations. Ideally, the model would be based on a culture calibration since the culture calibration represents the impact of only temperature on GDGT distributions. However, culture (Elling et al., 2015, 2017) and mesocosm (Schouten et al., 2007; Wuchter et al., 2004) studies show distinct differences with environmental calibrations (e.g., Kim et al., 2010) for reasons presently not clear. Since we are investigating sub-surface signals, we used the mean sub-surface $\text{TEX}_{86}^{\text{H}}$ calibration (Equations 11 and 12) as suggested by Ho and Laepple (2016) to obtain modelled TEX_{86} values, that is, the TEX_{86} values of the surface sediment reflecting the overall GDGT signal integrated from the overlying water column.

$$\text{modelled } \text{TEX}_{86}^{\text{H}} = \frac{T_{\text{model}} - 22.3}{40.8} \quad (11)$$

$$\text{modelled } \text{TEX}_{86} = 10^{(\text{modelled } \text{TEX}_{86}^{\text{H}})} \quad (12)$$

Nonetheless, the exact TEX_{86} -temperature calibration used here does not impact the conclusion of this modelling study.

3. Results

TEX_{86} , RI–OH, RI–OH' and $\text{U}_{37}^{\text{K}'}$ records from the deep and the shallow sites at the Chilean and the Angola margins are shown in Figure 2. The BIT values are <0.05 for all the samples from the Chilean and the Angola margins, which implies that no substantial terrestrial input reached these sites and should therefore not impact our TEX_{86} records to represent sea water temperature.

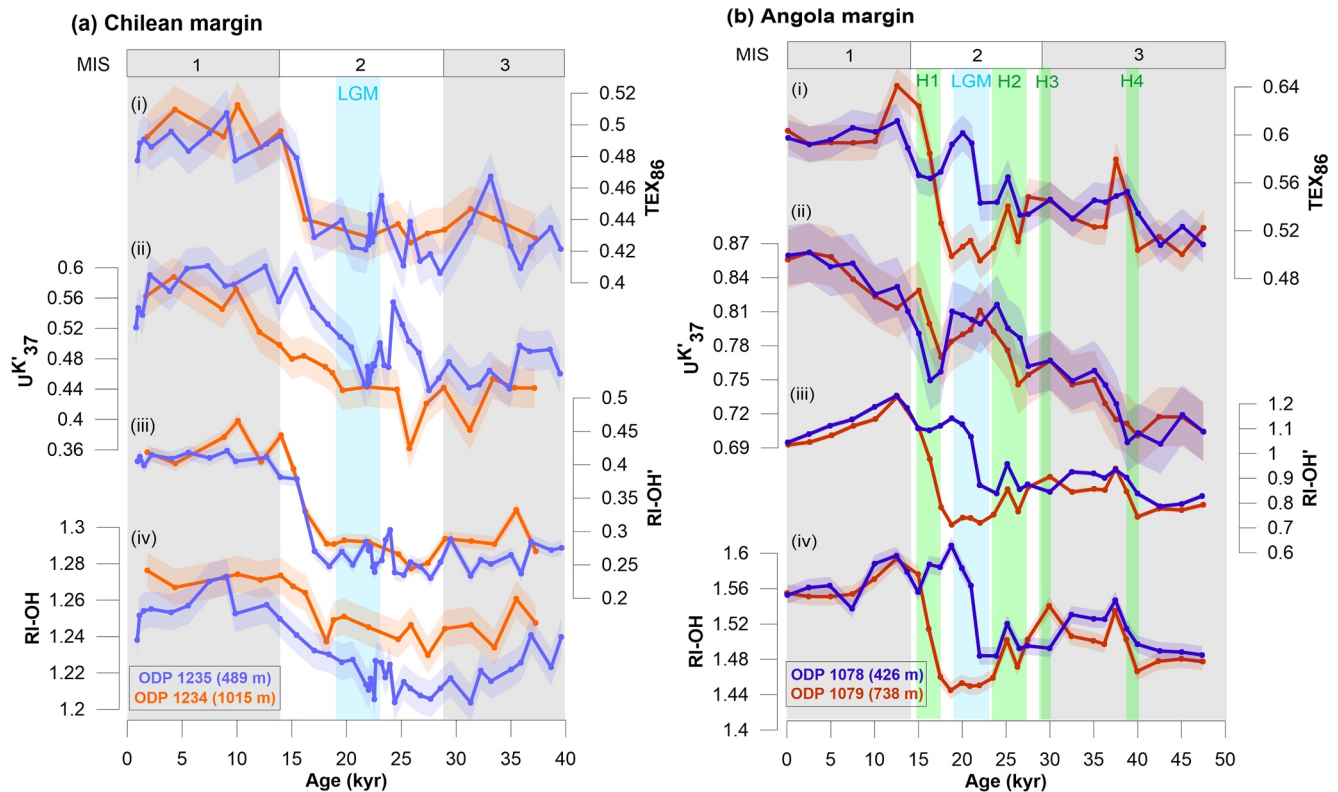


Figure 2. Paleothermometer results from the (a) Chilean and (b) Angola margins. Records from ODP Site 1234 from water depth of 1,015 m are in orange and ODP Site 1235 from water depth of 489 m are in violet. Records from ODP Site 1078 from water depth of 426 m are in purple and ODP Site 1079 from water depth of 738 m are in red. (i) TEX_{86} (ii) $U^{K'}_{37}$ (iii) $RI-OH'$ and (iv) $RI-OH$. Gray bars correspond to interglacial periods (Marine Isotope Stages, MIS 1 and 3). Blue bar indicates Last Glacial Maximum (LGM), and green bars indicate Heinrich Events. The shaded envelope around each record is the 1σ analytical uncertainty.

3.1. Chilean Margin

Between the deep and shallow sites at the Chilean margin, we observe overlapping records for TEX_{86} and $RI-OH'$, respectively (Figure 2a). Intriguingly, the $RI-OH$ values at the shallow site show consistently lower values compared to the $RI-OH$ at the deep site. The $U^{K'}_{37}$ proxy from the shallow site shows generally higher values between ~ 10 – 40 Kyr compared to the $U^{K'}_{37}$ proxy from the deep site.

The 2000-year binned data used to determine the correlation of proxy records between the shallow and the deep sites shows a high degree of correlation for TEX_{86} and $RI-OH'$ ($R^2 > 0.85$, $p < 0.001$), while $U^{K'}_{37}$ and $RI-OH$ shows a slightly lower correlation ($R^2 = 0.71$ and 0.73 , respectively; Figure 3a). The York regression trend also falls very close to the ordinary least squares fit (Figure 3a). A paired sample t -test was performed using the binned data to examine any difference between the same proxy signal carriers from the deep and the shallow sites at a significance level of 0.01. This showed that the mean of the differences between the deep and the shallow sites for TEX_{86} is not significantly different from zero, that is, the TEX_{86} record from deep and shallow sites does not statistically differ at the significance level of 0.01 (Table S2 in Supporting Information S1). In contrast, the $RI-OH'$, $RI-OH$ and $U^{K'}_{37}$ showed the mean of the differences between the sites to be significantly different from zero (Table S2 in Supporting Information S1).

The GDGT [2]/[3] record was also binned to 2000-year bins and a paired t -test was performed at a significance level of 0.01. The mean of the differences observed in the GDGT [2]/[3] ratios between the deep and the shallow site was significantly different from zero (Table S2 in Supporting Information S1).

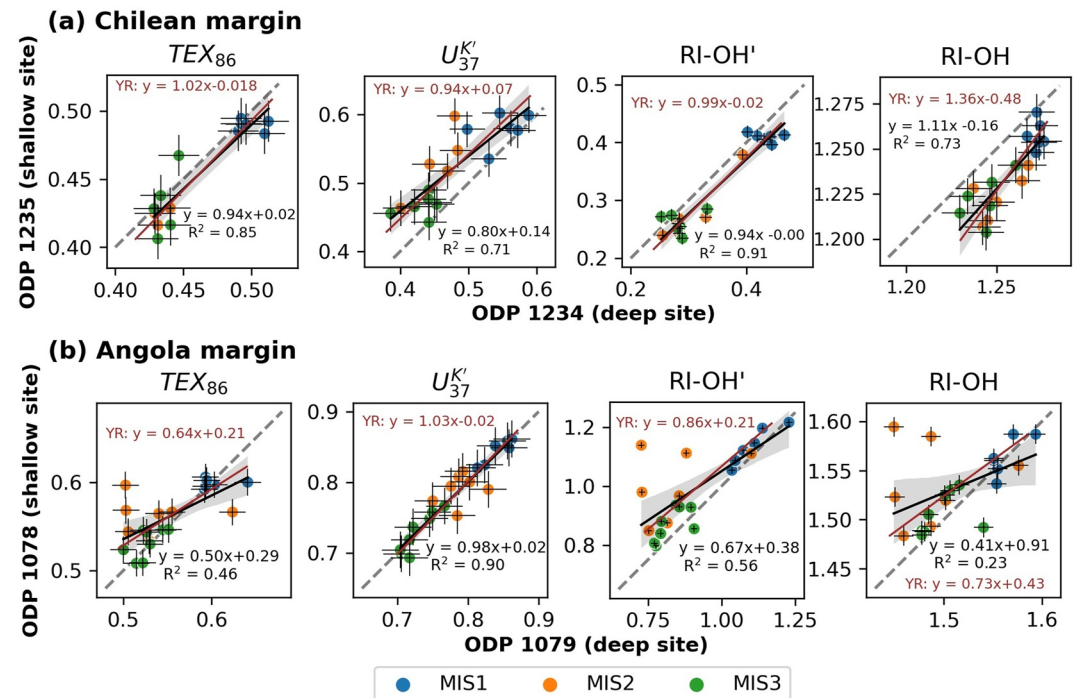


Figure 3. Cross-correlation between 2 Kyr-binned organic paleotemperature proxy values from deep versus shallow sites in (a) Chilean margin (water depths of 1,015 and 489 m, respectively) (b) Angola margin (water depths of 738 and 426 m, respectively). The x-axis denotes proxy values for the deep sites and y-axis for the shallow sites. Data points from Marine Isotope Stages, MIS 1, 2, 3 are in blue, orange, and green, respectively. Gray dashed lines are the 1:1 line. Linear regressions are indicated by black solid lines along with 95% confidence interval envelope. Brown solid lines denote the York regression (YR) trend for all samples. The error bars on the markers denote 1σ uncertainty of measurement.

3.2. Angola Margin

At the Angola margin, similar relationships between proxy values are observed when comparing deep and shallow sites, except during an interval from ~ 15 – 25 Kyr (Figure 2b). Interestingly, all the GDGT-based proxies, TEX₈₆, RI-OH' and RI-OH vary in a similar manner during the last deglaciation, with the shallow site showing a more gradual increase in proxy values compared to the deep site, which shows an abrupt and larger change in proxy values. We also observe an earlier increase in the TEX₈₆, RI-OH' and RI-OH proxy values indicating a deglacial warming trend at the shallow site (from ~ 23 Kyr) compared to the deep site where it begins at ~ 19 Kyr. The U₃₇^{K'} records from the deep and the shallow sites are in good agreement and also agree with previously reported U₃₇^{K'} values for ODP 1078 (Kim et al., 2003).

Similar to the Chilean record, binned data was used to determine the correlation of proxy records between the shallow and the deep sites. The U₃₇^{K'} proxy shows good correlation ($R^2 = 0.90$, $p < 0.001$) with the data points lying close to the 1:1 line (Figure 3b). However, TEX₈₆, RI-OH and RI-OH' show slightly lower correlations because of differences between proxy values during MIS 2. The York regression, which deals with errors in both x and y , shows a better fit, close to the 1:1 line (Figure 3b) as it gives small weights to large errors. The YR method is less affected by outliers than ordinary least squares (e.g., Mikkonen et al., 2019). A considerable improvement in the correlation between the deep and the shallow site records for TEX₈₆, RI-OH and RI-OH' proxies are observed (Figure S5 in Supporting Information S1) after removing the three data points in MIS 2 (orange data points corresponding to RI-OH' values >1 in Figure 3b). A paired sample t -test with the same binned data showed that the mean of the differences between the proxy values from the deep and the shallow sites is not significantly different from zero for U₃₇^{K'}, TEX₈₆ and RI-OH (Table S2 in Supporting Information S1). In contrast, RI-OH' shows the mean of the differences between the two sites to be significantly different from zero. The GDGT [2]/[3] ratio shows statistically significantly different records at the significance level of 0.01 between the deep and the shallow sites at this location (Table S2 in Supporting Information S1).

4. Discussion

To constrain the source depths for the various proxies considered, especially for the TEX_{86} , RI–OH and RI–OH', we compared the proxy values from the core pairs with each other, rather than the temperatures inferred from them or with $U_{37}^{K'}$ values. This avoids circular arguments associated with using pre-assigned temperature calibrations, which are tuned to specific depths (e.g., SST). We assume that the sedimentary records located close to each other with only water depth being different, received the same surface/sub-surface material from the overlying water column. In addition, the proxy records from the two sediment cores may be affected by differences in the depositional environment, which also may vary as a function of depth.

4.1. $U_{37}^{K'}$ Records

The $U_{37}^{K'}$ proxy is widely used to reconstruct SSTs and the depth of origin for alkenones is generally accepted to be the photic zone (e.g., Herbert et al., 1998; Müller et al., 1998; Popp et al., 2006; Ternois et al., 1996) although not necessarily the surface, as alkenones can be produced at depths up to 150 m (e.g., Ohkouchi et al., 1999; Prahl et al., 2005; Wolhowe et al., 2014). Hence, as a proof of concept, the $U_{37}^{K'}$ proxy, which thus should not be substantially impacted by differences in water depth above the sediment core, has been analysed in this study.

As expected, the $U_{37}^{K'}$ records from the Angola margin show good agreement between the deep and the shallow sites and are statistically indistinguishable, that is, within the error associated with the proxy analyses and the age uncertainty (Figure 2b). The $U_{37}^{K'}$ shows an increasing trend from ~ 27 Kyr towards the Last Glacial Maximum (LGM), while lower values are observed during Heinrich Events as indicated in Figure 2b. Kim et al. (2003) suggested strong south-east trade winds to the south of the Angola-Benguela Front (ABF) during the LGM, which enhanced transport of warm surface waters from the tropics brought in by the Angola Current (AC) to our study location. Conversely, during the Heinrich Events, weaker trade winds reduced the transport of warm waters by the AC. The observed close correlation between the $U_{37}^{K'}$ records from the deep and the shallow site and with the $U_{37}^{K'}$ record from Kim et al. (2003) reaffirms that the source signal of the $U_{37}^{K'}$ most likely comes from the surface waters.

Surprisingly, at the Chilean margin, the $U_{37}^{K'}$ at the shallow site reveals higher values compared to the deep site, except for the late Holocene and near LGM ~ 23 Kyr (Figure 2a). Since the alkenone source signal for $U_{37}^{K'}$ is thought to be mostly restricted to the photic zone, difference in water-mass distribution or upwelling would not cause a difference in $U_{37}^{K'}$ signal between such proximally (<12 km apart) located cores. A difference caused by upwelling waters would likely affect the $U_{37}^{K'}$ signals at both locations similarly. Post- and/or syn-depositional alterations of proxy signals could explain the observed difference. Although Site 1235 is a shallow site, contrary to our expectation, it has a lower total organic carbon (TOC) content, lower mass accumulation rates of organic carbon (average TOC ~ 0.6 and 1 wt%, for shallow and deep sites, respectively), and higher dilution by siliciclastics compared to the deep site (Mix et al., 2003; Muratli, Chase, Mix, & McManus, 2010; Prokopenko et al., 2006). The reason for elevated input of siliciclastic material in this area might be associated with discharges from the Bio-Bio or Itata river systems and also coastal erosion might have affected sediment deposition here (Muñoz et al., 2004; Muratli, Chase, McManus, & Mix, 2010). The difference in TOC and mass accumulation rates could have affected the biomarker preservation between the sites (Sinninghe Damsté, Rijpstra, et al., 2002). Additionally, sediment winnowing, which leads to preferential removal of fine-grained materials, is suggested for shallow site 1235 (Prokopenko et al., 2006), similar to what has been observed for other sites from the margins of Peru and southern Chile (Muñoz et al., 2004). Alkenones are shown to be preferentially associated with fine-grained mineral fraction (Ausín et al., 2021) and selective degradation of tri-unsaturated alkenones in coarser, low-surface area minerals would also bias $U_{37}^{K'}$ values, skewing this proxy towards warmer signals at Site 1235. However, grain-size analysis and more importantly, alkenone association with specific grain fractions are required to confirm this hypothesis. Additionally, a study near the Chilean margin shows admixing of older alkenones due to lateral transport in this area (Mollenhauer et al., 2005). Based on the observation of reworked benthic diatoms at the shallow site (Mix et al., 2003; Muñoz et al., 2004), a similar resuspension and advection process might be in play here. The extent to which selective preservation or lateral transport affects the alkenone signals at these sites causing an offset needs further investigation, for example, using compound-specific radiocarbon analysis (Mollenhauer et al., 2008).

4.2. TEX₈₆ Records

Comparison of the TEX₈₆ records between the two sites from the Chilean margin shows no major difference between them visually (Figure 2a), as well as statistically from the paired *t*-tests on the binned data. The fact that the TEX₈₆ does not show any significant offset between the sites at the Chilean margin, in contrast to the U₃₇^{K'}, is in line with observations that the GDGTs are less affected by lateral transport than alkenones (Mollenhauer et al., 2007; Shah et al., 2008). Also, selective degradation of GDGTs is less likely to affect TEX₈₆ records (Kim et al., 2009).

At the Angola margin, however, the TEX₈₆ record at the shallow site shows higher values compared to the deep site during a brief interval ~15–25 Kyr, and is similar to the trend of the U₃₇^{K'} records here (Figure 2b). In contrast, at the deep site, the TEX₈₆ record shows a larger change and a more abrupt deglaciation is observed. The δ¹⁸O values of benthic foraminifera at both these sites show a similar trend to the TEX₈₆ record from the deep site (Figure S4 in Supporting Information S1). Temperature changes based on ice-core data from the Antarctic shows a similar trend (Figure S4 in Supporting Information S1), which suggests a link to Antarctic climate, potentially via AAIW. A major contribution of AAIW to the water reaching the deep site during this period (~15–25 Kyr) could offset local TEX₈₆ values, provided part of the signal is produced at depths of AAIW. An increase in production of AAIW during the LGM has previously been suggested in other studies from the Southern Hemisphere (Martínez-Méndez et al., 2013; Muratli, Chase, Mix, & McManus, 2010; Wainer et al., 2012). Another mechanism that could contribute to a discrepancy between the deep and the shallow site could be a shift in production depth of Thaumarchaeota during ~15–25 Kyr. Still, the GDGT [2]/[3] ratios remain consistently high throughout the record at the deep site (Figure S4 in Supporting Information S1) which suggests that depth of production of the GDGTs also remained constant.

The GDGT [2]/[3] ratio was generally higher for the deep site compared to the shallow site, (Figures S3, S4 in Supporting Information S1), which is consistent with previous observations from other sites (e.g., Hernández-Sánchez et al., 2014; Kim et al., 2015; Taylor et al., 2013). Regardless of the brief interval showing an offset at the Angola Margin, for both sites, there is a strong similarity in the TEX₈₆ records between the core pairs, suggesting that the source signal is derived from the same water depth ranges. However, the GDGT [2]/[3] ratios between the deep and the shallow sites show statistically significant differences at both locations, which suggests a GDGT signal of potentially different archaeal communities from different water depths reached the underlying sediments. Comparing the TEX₈₆ and GDGT [2]/[3] ratio relationship for the deep and the shallow sites, we observe that the data points corresponding to the deep sites at both our study locations lie just at the edge of the temperature-dependent trend (data not shown) observed by Rattanasriampaipong et al. (2022). This suggests that some deeper water signal might be reaching the deep sites in these locations, but likely not to a great extent. Nevertheless, the TEX₈₆ is apparently not reflecting this difference.

To constrain the depth of the TEX₈₆ source signal, we modelled TEX₈₆ values as expected to be registered at our core sites using modern temperature-depth distributions and assuming different depth profiles of GDGT concentrations, based on modern ecology of Thaumarchaeota, with peak abundances set at different depths (see Methods and Supporting Information S1 for more detailed explanation). Furthermore, in order to keep the model simple, we assumed equal transport efficiency of GDGTs across all depths, although they may likely be biased towards the upper part of the water column (Wakeham et al., 2003; Wuchter et al., 2005). The modelled TEX₈₆ values calculated from abundance depth profiles of GDGTs with different peak abundance depths were compared between the pairs of cores (Figure 4). This comparison shows that, not surprisingly, if the TEX₈₆ is derived from shallow waters (e.g., maximum GDGT abundance at 50 m water depth), then predicted TEX₈₆ values are the same (on the 1:1 line) for shallow and deep sites. Values start to deviate from the 1:1 line when the maximum GDGT abundance is around 300–350 m (Figure 4), which means that if the TEX₈₆ source signal is from depths deeper than this, then we expect an offset in TEX₈₆ values between deep and shallow sites.

When we plot measured TEX₈₆ values (binned data points from Figure 3) from MIS 1, representing similar conditions as present against the modelled values, we see that they fall very close to the same 1:1 line (Figure 4), especially for the data points from the most recent time periods. This supports the notion that the source signal of TEX₈₆ must be derived from depths shallower than 350 m at both locations.

Our conclusions are in line with previous SPM studies from the South Atlantic, which show that the majority of the sedimentary GDGT signal comes from sub-surface waters of 80–250 m depths (Hernández-Sánchez et al., 2014; Hurley et al., 2016, 2018). However, regional differences are suggested from several studies from various locations. Basse et al. (2014) observed that the major contribution of GDGTs to the sediments in the

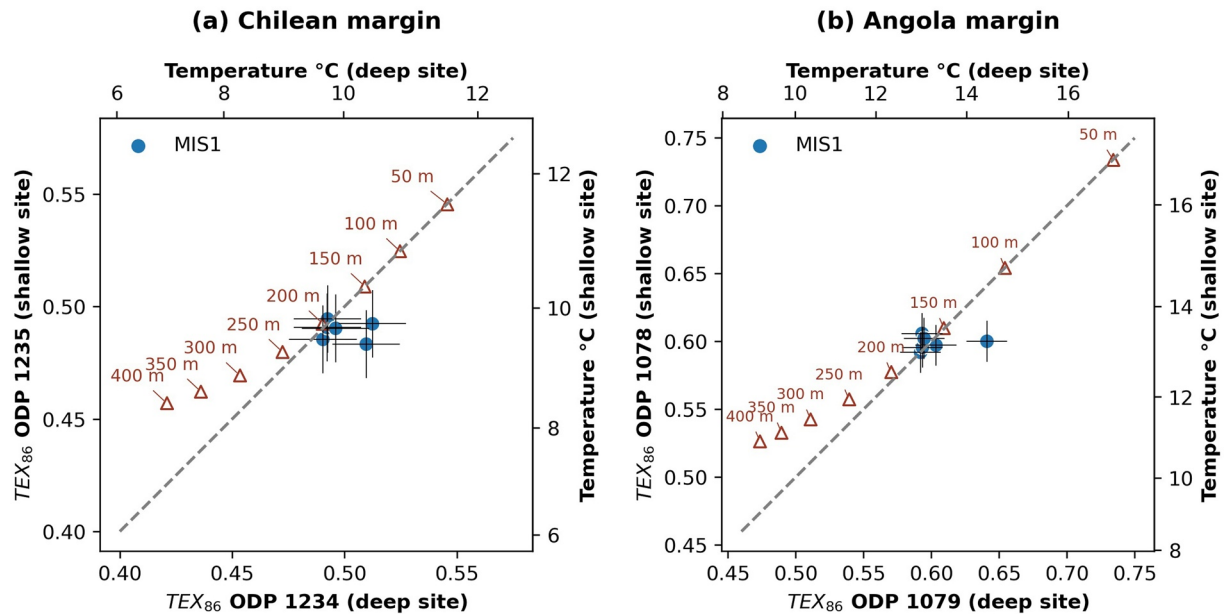


Figure 4. Comparison of measured and modelled TEX_{86} (or modelled temperature) values at deep versus shallow sites for (a) Chilean margin (water depths of 1,015 and 489 m, respectively) and (b) Angola margin (water depths of 738 and 426 m, respectively). Open triangles in brown represent the modelled TEX_{86} (or modelled temperature) values with its corresponding water depth maxima of GDGT abundance. Gray dashed line indicates the 1:1 line. Data points from MIS 1 are in blue. The error bars on the markers denote 1σ uncertainty of measurement.

upwelling region in the NW Africa is coming from surface waters and the contribution from the oxygen minimum zone (300–600 m) is probably only minor. Surface sediment and SPM studies from the East China Sea suggest TEX_{86}^H reflects bottom water (<100 m depth) temperatures (Guo et al., 2021; Wang et al., 2019). GDGT contributions from >500 m from deep water Thaumarchaeotal communities are observed in the Mediterranean and near the Portugal margin influenced by deep Mediterranean Outflow Waters (Besseling et al., 2019; Kim et al., 2015, 2016). For the Southern Ocean, it has been suggested that a significant amount of GDGTs from depths of >1,400 m might be reaching the underlying sediments (Spencer-Jones et al., 2021). Hence, regional studies are required to constrain the source depth of the TEX_{86} signal at different locations. Our approach of using closely located cores from different water depths may provide a solution to this problem, potentially also for older sedimentary records.

4.3. OH-GDGT Based Proxies

At both locations, TEX_{86} and RI–OH' mostly vary synchronously (Figure 2). The RI–OH and RI–OH' records from the Angola margin show similar trends to the TEX_{86} records at this location, even during the brief interval ~15–25 Kyr, where a deviation between the deep and the shallow site is observed in the TEX_{86} signal (Figure 2b). This suggests a common source, and thus a common export depth for iGDGTs and OH-GDGTs. Indeed, several studies suggested the same source organisms for iGDGTs and OH-GDGTs, namely Group I.1a Thaumarchaeota (Elling et al., 2014, 2015, 2017; Sinninghe Damsté et al., 2012, 2022).

Interestingly, a systematic offset between the RI–OH records in the deep and the shallow site is observed for the Chilean margin which is not observed in the corresponding RI–OH' records (Figure 2a). The most likely explanation for the offset seen in the RI–OH proxy record is that the RI–OH does not fully incorporate the temperature changes at this location. The dominant OH-GDGT in moderate and low temperature regions is OH-GDGT-0 (C. Huguet et al., 2013) which is also the case here with an average relative abundance of around 74%. The average contribution from OH-GDGT-1 and -2 is 20% and 7%, respectively, which means that the RI–OH proxy (which does not have OH-GDGT-0 in its definition- Equation 5) is mainly controlled by the abundance of OH-GDGT-1 here. OH-GDGT-1 is known to behave differently compared to other OH-GDGTs in the Chinese coastal seas (Lü et al., 2015) where its relative abundance decreases going from coastal to offshore sites. This could suggest that the OH-GDGT-1 is impacted by factors other than temperature. Hence, our results suggest that the RI–OH' might be better suited to derive a temperature signal with OH-GDGTs than RI–OH.

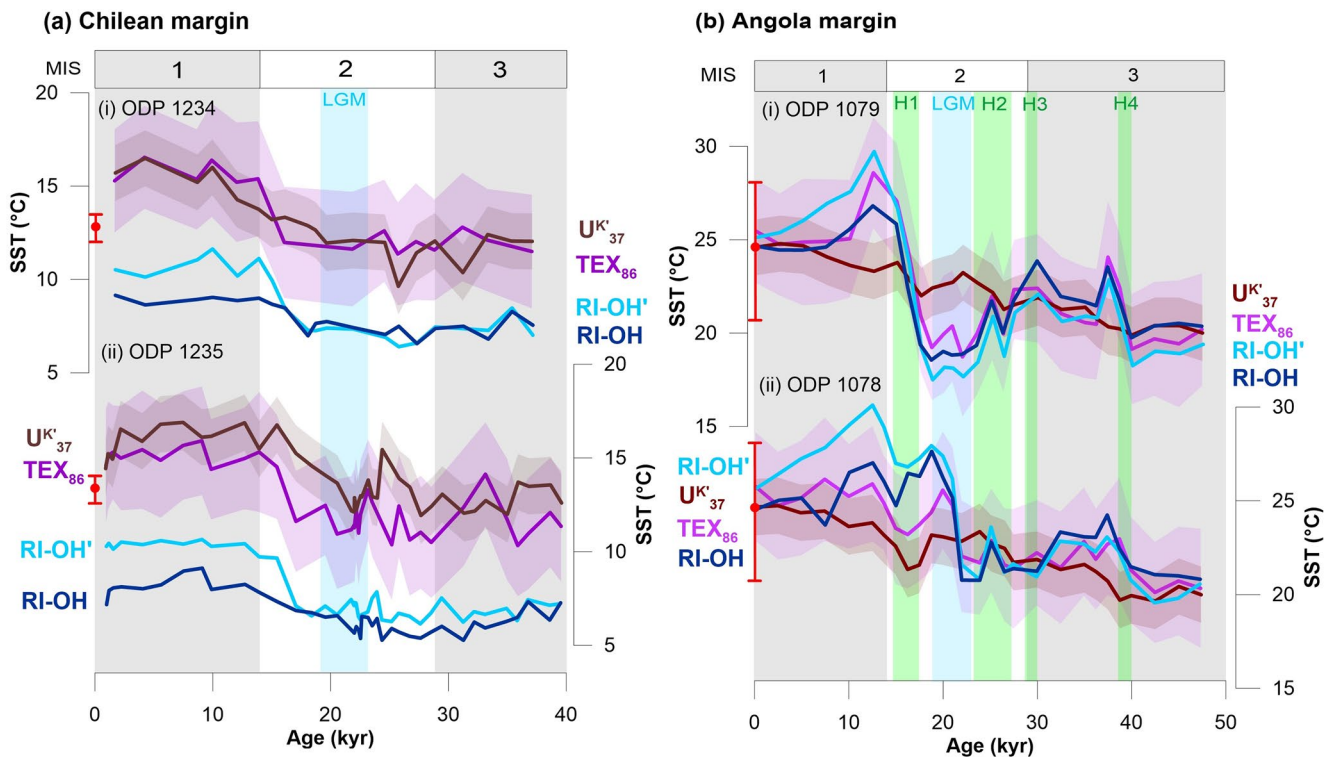


Figure 5. Organic proxy temperature reconstruction from the (a) Chilean and (b) Angola margins based on $U_{37}^{K'}$, TEX_{86} , RI-OH and RI-OH'. The red symbols with bars denote the modern mean annual temperature with the seasonal range at this location (Locarnini et al., 2019). The shaded envelopes around TEX_{86} records denotes 1σ uncertainty in BAYSPAR TEX_{86} -SST for each location ($\sim 3^{\circ}C$) (Tierney & Tingley, 2014, 2015) and around $U_{37}^{K'}$ records (Müller et al., 1998) ($1.5^{\circ}C$ uncertainty). For RI-OH and RI-OH', the standard deviation for residuals is $\sim 6^{\circ}C$ (Lü et al., 2015) (not shaded here).

4.4. Temperature Reconstructions

Now that we have constrained the different source depths, we can convert our proxy records into temperature estimates. Clearly, for the $U_{37}^{K'}$ we can use a calibration against SST (Equation 2 according to Müller et al., 1998). For the TEX_{86} , different surface and sub-surface temperature calibrations exist, that is, the BAYSPAR SST calibration (Tierney & Tingley, 2014, 2015), TEX_{86}^H calibration with SST (Kim et al., 2010), and regional calibrations (e.g., Kaiser et al. (2015) for Chilean records) and the mean of the ensemble TEX_{86}^H sub-surface reformulation suggested by Ho and Laepple (2016) (Figure S2 in Supporting Information S1). Although our results do not exclude a sub-surface origin of the signal, we used the BAYSPAR SST calibration for TEX_{86} to examine whether our TEX_{86} signal could reflect SST, assuming that a strong correlation between surface and sub-surface temperatures exists in our study locations over time. Similarly, for OH-GDGT based proxies, we used the latest SST calibration according to Lü et al. (2015) and Fietz et al. (2020) (Equations 7 and 8).

The modern mean annual SST recorded of the Chilean margin sites is $13^{\circ}C$ (Locarnini et al., 2019), which is close to the most recent temperature values as indicated by the TEX_{86} values (15.4 and $14.6^{\circ}C$ for deep and shallow sites, respectively) and the $U_{37}^{K'}$ values (14.7 and $14.5^{\circ}C$ for the deep and the shallow sites, respectively), that is, within the proxy uncertainty of ~ 3 and $1.5^{\circ}C$, respectively (Figure 5a). Comparing temperature estimates for the LGM, the average $U_{37}^{K'}$ SST estimates are around 12 and $12.9^{\circ}C$ for the deep and the shallow site, respectively, which is close to the TEX_{86} SST values of 11.7 and $11.6^{\circ}C$ for the deep and the shallow site, respectively, also well within the proxy error limits. This suggests that the TEX_{86} -SST relationship is also applicable for the LGM at this location. In contrast, the uppermost samples give much lower temperature estimates based on OH-GDGT proxies compared to the actual modern annual mean SST, that is, estimates of 10.9 and $10.3^{\circ}C$ for deep and shallow sites, respectively, from RI-OH' and 9 and $7.1^{\circ}C$ for deep and shallow sites, respectively, from RI-OH. Similarly, during the LGM, the RI-OH' (with 7.5 and $6.9^{\circ}C$ for deep and shallow sites, respectively) and RI-OH (with 7.7 and $5.9^{\circ}C$ for deep and shallow sites, respectively) based temperature estimates indicate much lower temperatures compared to the $U_{37}^{K'}$ based SST estimates. A seasonal bias to

winter with deep convective mixing which happens consistently throughout the record for OH-GDGT based proxies compared to other paleothermometers is unlikely since the reconstructed temperature is much below the modern austral winter SST of around 12°C (Locarnini et al., 2019) at this location. A systematic depth bias of OH-GDGT contribution from deeper depths to reflect colder temperatures at both the locations may be an alternative explanation, though this would be contrary to the idea that OH-GDGTs are derived from similar depths as non-hydroxylated iGDGTs (e.g., Fietz et al., 2013; Sinninghe Damsté et al., 2012, 2022). Furthermore, as discussed in Section 4.3, a similar export depth of GDGTs and OH-GDGTs was concluded based upon concurrent records of TEX₈₆ and OH-GDGT based proxies. Although the calibration uncertainties for RI–OH and RI–OH' are large (~6°C) (Fietz et al., 2020; Lü et al., 2015), they show a clear glacial-interglacial temperature variability like other proxies, which suggest a need for better global or regional temperature calibrations for OH-GDGT based proxies.

At the Angola margin, all temperature proxies measured in the uppermost sample at both the deep and the shallow sites are within the proxy error of annual mean SST of 24.8°C (Locarnini et al., 2019) (Figure 5). The TEX₈₆ values for the deep and the shallow sites, respectively, are 25.5 and 25.8°C. The RI–OH' gives similar temperature values of 25.2 and 25.7°C for deep and shallow sites, respectively. The U₃₇^{K'} gives much closer values of 24.6 and 24.7°C and so does RI–OH with 24.7 and 24.5°C for deep and shallow sites, respectively. The average U₃₇^{K'} SST estimates during LGM for the deep and the shallow sites are around 22.9 and 23°C, respectively, which are close to the temperature estimates from other proxies from the shallow site (TEX₈₆ SST of 24.1°C, RI–OH' SST of 25.1°C and RI–OH SST of 24°C). In contrast, the deep site gives much lower SST estimates at the LGM for TEX₈₆, RI–OH' and RI–OH (19.8, 18.1 and 19°C, respectively), which is probably due to the influence of colder intermediate waters at this site as discussed above.

The general agreement between TEX₈₆ and U₃₇^{K'} records suggest that the TEX₈₆ could still reasonably predict SST at these locations, as long as there are no changes in water mass characteristics at depth (like possibly at the Angola margin during ~15–25 Kyr, see above). It should be noted though that alkenone production is known to occur in deeper thermocline waters in certain locations (e.g., Ohkouchi et al., 1999; Popp et al., 2006) and thus the U₃₇^{K'} reflects a temperature signal from a depth range rather than sea surface (0 m), albeit a narrower range than what TEX₈₆ reflects. In contrast to the TEX₈₆ and U₃₇^{K'}, the reconstructed temperatures from RI–OH' and RI–OH proxies largely disagree with the temperature range indicated by other proxy records, especially at the Chilean margin. The RI–OH' and RI–OH have been shown to be promising temperature proxies in several regions, for example, at the Iberian margin, the Chinese coastal seas, the Mediterranean Sea, the Southern Ocean (e.g., Davtian et al., 2019, 2021; Lamping et al., 2021; Lü et al., 2015; Yang et al., 2018). However, in the global calibration (Fietz et al., 2020; Lü et al., 2015), the large scatter in data points likely indicates regional differences in the response of the OH-GDGT signal to temperature or an impact of non-thermal factors. More regional studies from different locations and a comprehensive examination of the global data set need to be done to better constrain the applicability of OH-GDGT based proxies.

5. Conclusions

Two marine sediment cores in close proximity, but retrieved from different water depths, from the Chilean and the Angola margin were studied to constrain the depth origin of organic paleothermometers in sedimentary archives. As expected, the U₃₇^{K'} reflects sea surface temperature, but the proxy signal may be impacted by post-depositional changes or lateral transport even for closely located cores. The statistically indistinguishable TEX₈₆ records at each of these locations as well as modelling results suggest that the source signal of the TEX₈₆ proxy is derived from depths <350 m at our study locations. Though the TEX₈₆ source signal is likely coming from sub-surface depths, a good correlation between surface and sub-surface temperature variations would still allow us to use TEX₈₆ for SST reconstructions (cf. Huber, 2010; J. E. Tierney, 2013). However, changes in ocean dynamics and sea-level changes, especially during glacial periods might lead to variations in intensity and/or contribution of different water masses to a particular location, which could affect the agreement between surface and sub-surface temperatures and hence, the TEX₈₆ SST estimates. Although similar trends in TEX₈₆ and OH-GDGT based proxies point towards similar source depths for these proxies, further studies are required to constrain OH-GDGT based proxies to obtain better absolute temperature estimations from them. Our results show that proximally located cores from different water depths can be used to potentially constrain the export depth of organic proxies.

Data Availability Statement

All data is available online at PANGAEA repository (Hättig et al., 2023; Varma et al., 2023).

Acknowledgments

This research used samples and data provided by the International Ocean Discovery Program (IODP). We thank Holger Kuhlmann from Bremen ODP Core Repository for providing samples from Site 1078 and 1079 and Michelle Penkrot from Gulf Coast Repository for samples from Site 1235. Marijke de Bar is thanked for the results from Site 1234. Anhelique Mets, Monique Verweij, Denise Dorhout and Ellen Hopmans are thanked for analytical support. Thanks to MICADAS radiocarbon laboratory at Alfred Wegener Institute (AWI), Bremerhaven, for radiocarbon analysis. We thank the three anonymous reviewers for their constructive comments. This work was carried out under the umbrella of the Netherlands Earth System Science Centre (NESSC). This project has received funding from the European Union's Horizon 2020 research and innovation programme under the Marie Skłodowska-Curie, grant agreement No 847504.

References

- Allaart, L., Müller, J., Schomacker, A., Rydningen, T. A., Håkansson, L., Kjellman, S. E., et al. (2020). Late Quaternary glacier and sea-ice history of northern Wijdefjorden, Svalbard. *Boreas*, 49(3), 417–437. <https://doi.org/10.1111/BOR.12435>
- Ausin, B., Haghipour, N., Bruni, E., & Eglinton, T. (2021). The influence of lateral transport on sedimentary alkenone paleoproxy signals. *Biogeochemistry Discussions*, 1–25. <https://doi.org/10.5194/BG-2021-204>
- Bale, N. J., Palatinszky, M., Rijpsma, W. I. C., Herbold, C. W., Wagner, M., & Damsté, J. S. S. (2019). Membrane lipid composition of the moderately thermophilic ammonia-oxidizing archaeon “Candidatus Nitrosotenuis uzonensis” at different growth temperatures. *Applied and Environmental Microbiology*, 85(20). <https://doi.org/10.1128/AEM.01332-19>
- Basse, A., Zhu, C., Versteegh, G. J. M., Fischer, G., Hinrichs, K. U., & Mollenhauer, G. (2014). Distribution of intact and core tetraether lipids in water column profiles of suspended particulate matter off Cape Blanc, NW Africa. *Organic Geochemistry*, 72, 1–13. <https://doi.org/10.1016/j.orggeochem.2014.04.007>
- Bentaleb, I., Fontugne, M., & Beaufort, L. (2002). Long-chain alkenones and U37k' variability along a South–North transect in the Western Pacific Ocean. *Global and Planetary Change*, 34(3–4), 173–183. [https://doi.org/10.1016/S0921-8181\(02\)00113-3](https://doi.org/10.1016/S0921-8181(02)00113-3)
- Besseling, M. A., Hopmans, E. C., Bale, N. J., Schouten, S., Damsté, J. S. S., & Villanueva, L. (2020). The absence of intact polar lipid-derived GDGTs in marine waters dominated by Marine Group II: Implications for lipid biosynthesis in Archaea. *Scientific Reports*, 10(1), 294. <https://doi.org/10.1038/S41598-019-57035-0>
- Besseling, M. A., Hopmans, E. C., Koenen, M., van der Meer, M. T. J., Vreugdenhil, S., Schouten, S., et al. (2019). Depth-related differences in archaeal populations impact the isoprenoid tetraether lipid composition of the Mediterranean Sea water column. *Organic Geochemistry*, 135, 16–31. <https://doi.org/10.1016/j.orggeochem.2019.06.008>
- Blaauw, M., & Christeny, J. A. (2011). Flexible paleoclimate age-depth models using an autoregressive gamma process. *Bayesian Analysis*, 6(3), 457–474. <https://doi.org/10.1214/11-BA618>
- Church, M. J., Wai, B., Karl, D. M., & DeLong, E. F. (2010). Abundances of crenarchaeal *amoA* genes and transcripts in the Pacific Ocean. *Environmental Microbiology*, 12(3), 679–688. <https://doi.org/10.1111/j.1462-2920.2009.02108.x>
- Davtian, N., Bard, E., Darfeuil, S., Ménot, G., & Rostek, F. (2021). The novel hydroxylated tetraether index RI-OH' as a sea surface temperature proxy for the 160–45 ka BP period off the Iberian margin. *Paleoceanography and Paleoclimatology*, 36(3), 1–34. <https://doi.org/10.1029/2020PA004077>
- Davtian, N., Ménot, G., Fagault, Y., & Bard, E. (2019). Western Mediterranean Sea paleothermometry over the Last Glacial cycle based on the novel RI-OH index. *Paleoceanography and Paleoclimatology*, 34(4), 616–634. <https://doi.org/10.1029/2018PA003452>
- de Bar, M. W., Rampen, S. W., Hopmans, E. C., Sinninghe Damsté, J. S., & Schouten, S. (2019). Constraining the applicability of organic paleotemperature proxies for the last 90 Myrs. *Organic Geochemistry*, 128, 122–136. <https://doi.org/10.1016/j.orggeochem.2018.12.005>
- de Bar, M. W., Stolwijk, D. J., McManus, J. F., Sinninghe Damsté, J. S., & Schouten, S. (2018). A late quaternary climate record based on long-chain diol proxies from the Chilean margin. *Climate of the Past*, 14(11), 1783–1803. <https://doi.org/10.5194/cp-14-1783-2018>
- De Jonge, C., Stadnitskaia, A., Hopmans, E. C., Cherkashov, G., Fedotov, A., Streletskaia, I. D., et al. (2015). Drastic changes in the distribution of branched tetraether lipids in suspended matter and sediments from the Yenisei River and Kara Sea (Siberia): Implications for the use of brGDGT-based proxies in coastal marine sediments. *Geochimica et Cosmochimica Acta*, 165, 200–225. <https://doi.org/10.1016/j.gca.2015.05.044>
- Dupont, L. M., Behling, H., & Kim, J. H. (2008). Thirty thousand years of vegetation development and climate change in Angola (Ocean Drilling Program Site 1078) (Climate of the Past (2008) 4 (107–124)). *Climate of the Past*, 4(1), 107–124. <https://doi.org/10.5194/cp-7-115-2011>
- Elling, F. J., Könneke, M., Lipp, J. S., Becker, K. W., Gagen, E. J., & Hinrichs, K. U. (2014). Effects of growth phase on the membrane lipid composition of the thaumarchaeon *Nitrosopumilus maritimus* and their implications for archaeal lipid distributions in the marine environment. *Geochimica et Cosmochimica Acta*, 141, 579–597. <https://doi.org/10.1016/j.gca.2014.07.005>
- Elling, F. J., Könneke, M., Mußmann, M., Greve, A., & Hinrichs, K. U. (2015). Influence of temperature, pH, and salinity on membrane lipid composition and TEX86 of marine planktonic thaumarchaeal isolates. *Geochimica et Cosmochimica Acta*, 171, 238–255. <https://doi.org/10.1016/j.gca.2015.09.004>
- Elling, F. J., Könneke, M., Nicol, G. W., Stieglmeier, M., Bayer, B., Spieck, E., et al. (2017). Chemotaxonomic characterisation of the thaumarchaeal lipidome. *Environmental Microbiology*, 19(7), 2681–2700. <https://doi.org/10.1111/1462-2920.13759>
- Fietz, S., Ho, S. L., & Hugué, C. (2020). Archaeal membrane lipid-based paleothermometry for applications in polar oceans. *Oceanography*, 33(2), 105–114. <https://doi.org/10.5670/oceanog.2020.207>
- Fietz, S., Hugué, C., Rueda, G., Hambach, B., & Rosell-Melé, A. (2013). Hydroxylated isoprenoid GDGTs in the Nordic Seas. *Marine Chemistry*, 152, 1–10. <https://doi.org/10.1016/j.marchem.2013.02.007>
- Francis, C. A., Roberts, K. J., Beman, J. M., Santoro, A. E., & Oakley, B. B. (2005). Ubiquity and diversity of ammonia-oxidizing archaea in water columns and sediments of the ocean. *Proceedings of the National Academy of Sciences*, 102(41), 14683–14688. <https://doi.org/10.1073/PNAS.0506625102>
- Guo, J., Yuan, H., Song, J., Qu, B., Xing, J., Wang, Q., et al. (2021). Variation of isoprenoid GDGTs in the stratified marine water column: Implications for GDGT-based TEX86 paleothermometry. *Frontiers in Marine Science*, 8(August), 1–11. <https://doi.org/10.3389/fmars.2021.715708>
- Hättig, K., Varma, D., van der Meer Marcel, T. J., Reichart, G.-J., & Schouten, S. (2023). Age model for ODP Leg 202 site 1235 and site 1234. [Dataset]. PANGAEA. <https://doi.org/10.1594/PANGAEA.957070>
- Hebbeln, D., Marchant, M., Freudenthal, T., & Wefer, G. (2000). Surface sediment distribution along the Chilean continental slope related to upwelling and productivity. *Marine Geology*, 164(3–4), 119–137. [https://doi.org/10.1016/S0025-3227\(99\)00129-2](https://doi.org/10.1016/S0025-3227(99)00129-2)
- Herbert, T. D., Schuffert, J. D., Thomas, D., Lange, C., Weinheimer, A., Peleo-Alampay, A., & Herguera, J. C. (1998). Depth and seasonality of alkenone production along the California margin inferred from a core top transect. *Paleoceanography*, 13(3), 263–271. <https://doi.org/10.1029/98PA00069>
- Hernández-Sánchez, M. T., Woodward, E. M. S., Taylor, K. W. R., Henderson, G. M., & Pancost, R. D. (2014). Variations in GDGT distributions through the water column in the South East Atlantic Ocean. *Geochimica et Cosmochimica Acta*, 132, 337–348. <https://doi.org/10.1016/j.gca.2014.02.009>

- Herndl, G. J., Reinthaler, T., Teira, E., Van Aken, H., Veth, C., Perntaler, A., & Perntaler, J. (2005). Contribution of Archaea to total prokaryotic production in the deep Atlantic Ocean. *Applied and Environmental Microbiology*, 71(5), 2303–2309. <https://doi.org/10.1128/AEM.71.5.2303-2309.2005>
- Hines, B. R., Hollis, C. J., Atkins, C. B., Baker, J. A., Morgans, H. E. G., & Strong, P. C. (2017). Reduction of oceanic temperature gradients in the early Eocene Southwest Pacific Ocean. *Palaeoecography, Palaoclimatology, Palaeoecology*, 475, 41–54. <https://doi.org/10.1016/j.palaeo.2017.02.037>
- Ho, S. L., & Laepple, T. (2016). Flat meridional temperature gradient in the early Eocene in the subsurface rather than surface ocean. *Nature Geoscience*, 9(8), 606–610. <https://doi.org/10.1038/ngeo2763>
- Hopmans, E. C., Schouten, S., & Sinninghe Damsté, J. S. (2016). The effect of improved chromatography on GDGT-based palaeoproxies. *Organic Geochemistry*, 93, 1–6. <https://doi.org/10.1016/j.orggeochem.2015.12.006>
- Hopmans, E. C., Weijers, J. W. H., Schefuß, E., Herfort, L., Sinninghe Damsté, J. S., & Schouten, S. (2004). A novel proxy for terrestrial organic matter in sediments based on branched and isoprenoid tetraether lipids. *Earth and Planetary Science Letters*, 224(1–2), 107–116. <https://doi.org/10.1016/j.epsl.2004.05.012>
- Hu, A., Jiao, N., & Zhang, C. L. (2011). Community structure and function of planktonic crenarchaeota: Changes with depth in the South China Sea. *Microbial Ecology*, 62(3), 549–563. <https://doi.org/10.1007/S00248-011-9866-Z>
- Huber, M. (2010). Why improving molecular and isotopic proxy paleoclimate records is the most important problem in science today: A climate modeling perspective. In *Gordon research conference*. Retrieved from https://scholar.google.com/scholar_lookup?author=M.%20Huber&inst=7240083048524121927&publication_year=2010&title=Why%20improving%20molecular%20and%20isotopic%20proxy%20paleoclimate%20records%20is%20the%20most%20important%20problem%20in%20science%20today%3A%20A%20climate%20modeling%20perspective
- Huguet, C., Fietz, S., & Rosell-Melé, A. (2013). Global distribution patterns of hydroxy glycerol dialkyl glycerol tetraethers. *Organic Geochemistry*, 57, 107–118. <https://doi.org/10.1016/j.orggeochem.2013.01.010>
- Huguet, C., Schimmelmann, A., Thunell, R., Lourens, L. J., Damsté, J. S. S., & Schouten, S. (2007). A study of the TEX86 paleothermometer in the water column and sediments of the Santa Barbara Basin, California. *Paleoceanography*, 22(3), 3203. <https://doi.org/10.1029/2006PA001310>
- Hurler, S. J., Elling, F. J., Könneke, M., Buchwald, C., Wankel, S. D., Santoro, A. E., et al. (2016). Influence of ammonia oxidation rate on thaumarchaeal lipid composition and the TEX86 temperature proxy. *Proceedings of the National Academy of Sciences of the United States of America*, 113(28), 7762–7767. <https://doi.org/10.1073/pnas.1518534113>
- Hurler, S. J., Lipp, J. S., Close, H. G., Hinrichs, K. U., & Pearson, A. (2018). Distribution and export of isoprenoid tetraether lipids in suspended particulate matter from the water column of the Western Atlantic Ocean. *Organic Geochemistry*, 116, 90–102. <https://doi.org/10.1016/j.orggeochem.2017.11.010>
- Jenkyns, H. C., Forster, A., Schouten, S., & Sinninghe Damsté, J. S. (2004). High temperatures in the Late Cretaceous Arctic Ocean. *Nature*, 432(7019), 888–892. <https://doi.org/10.1038/NATURE03143>
- Jenkyns, H. C., Schouten-Huibers, L., Schouten, S., & Sinninghe Damsté, J. S. (2012). Warm Middle Jurassic–Early Cretaceous high-latitude sea-surface temperatures from the Southern Ocean. *Climate of the Past*, 8(1), 215–225. <https://doi.org/10.5194/cp-8-215-2012>
- Jia, G., Zhang, J., Chen, J., Peng, P., & Zhang, C. L. (2012). Archaeal tetraether lipids record subsurface water temperature in the South China Sea. *Organic Geochemistry*, 50, 68–77. <https://doi.org/10.1016/j.orggeochem.2012.07.002>
- Kaiser, J., Schouten, S., Kilian, R., Arz, H. W., Lamy, F., & Sinninghe Damsté, J. S. (2015). Isoprenoid and branched GDGT-based proxies for surface sediments from marine, fjord and lake environments in Chile. *Organic Geochemistry*, 89(90), 117–127. <https://doi.org/10.1016/j.orggeochem.2015.10.007>
- Karner, M. B., Delong, E. F., & Karl, D. M. (2001). Archaeal dominance in the mesopelagic zone of the Pacific Ocean. *Nature*, 409(6819), 507–510. <https://doi.org/10.1038/35054051>
- Kim, J. H., Huguet, C., Zonneveld, K. A. F., Versteegh, G. J. M., Roeder, W., Sinninghe Damsté, J. S., & Schouten, S. (2009). An experimental field study to test the stability of lipids used for the TEX86 and U37K' palaeothermometers. *Geochimica et Cosmochimica Acta*, 73(10), 2888–2898. <https://doi.org/10.1016/J.GCA.2009.02.030>
- Kim, J. H., Schneider, R. R., Multiza, S., & Müller, P. J. (2003). Reconstruction of SE trade-wind intensity based on sea-surface temperature gradients in the Southeast Atlantic over the last 25 kyr. *Geophysical Research Letters*, 30(22), 3–6. <https://doi.org/10.1029/2003GL017557>
- Kim, J. H., Schouten, S., Rodrigo-Gámiz, M., Rampen, S., Marino, G., Huguet, C., et al. (2015). Influence of deep-water derived isoprenoid tetraether lipids on the TEX86H paleothermometer in the Mediterranean Sea. *Geochimica et Cosmochimica Acta*, 150, 125–141. <https://doi.org/10.1016/j.gca.2014.11.017>
- Kim, J. H., van der Meer, J., Schouten, S., Helmke, P., Willmott, V., Sangiorgi, F., et al. (2010). New indices and calibrations derived from the distribution of crenarchaeal isoprenoid tetraether lipids: Implications for past sea surface temperature reconstructions. *Geochimica et Cosmochimica Acta*, 74(16), 4639–4654. <https://doi.org/10.1016/j.gca.2010.05.027>
- Kim, J. H., Villanueva, L., Zell, C., & Sinninghe Damsté, J. S. (2016). Biological source and provenance of deep-water derived isoprenoid tetraether lipids along the Portuguese continental margin. *Geochimica et Cosmochimica Acta*, 172, 177–204. <https://doi.org/10.1016/j.gca.2015.09.010>
- Kopte, R., Brandt, P., Dengler, M., Tchupalanga, P. C. M., Macuéria, M., & Ostrowski, M. (2017). The Angola Current: Flow and hydrographic characteristics as observed at 11°S. *Journal of Geophysical Research: Oceans*, 122(2), 1177–1189. <https://doi.org/10.1002/2016JC012374>
- Kremer, A., Stein, R., Fahl, K., Ji, Z., Yang, Z., Wiers, S., et al. (2018). Changes in sea ice cover and ice sheet extent at the Yermak Plateau during the last 160 ka – Reconstructions from biomarker records. *Quaternary Science Reviews*, 182, 93–108. <https://doi.org/10.1016/j.quascirev.2017.12.016>
- Lamping, N., Müller, J., Hefter, J., Mollenhauer, G., Haas, C., Shi, X., et al. (2021). Evaluation of lipid biomarkers as proxies for sea ice and ocean temperatures along the Antarctic continental margin. *Climate of the Past*, 17(5), 2305–2326. <https://doi.org/10.5194/cp-17-2305-2021>
- Lipp, J. S., & Hinrichs, K. U. (2009). Structural diversity and fate of intact polar lipids in marine sediments. *Geochimica et Cosmochimica Acta*, 73(22), 6816–6833. <https://doi.org/10.1016/j.gca.2009.08.003>
- Liu, X.-L., Lipp, J. S., Simpson, J. H., Lin, Y. S., Summons, R. E., & Hinrichs, K. U. (2012). Mono- and dihydroxyl glycerol dibiphytanyl glycerol tetraethers in marine sediments: Identification of both core and intact polar lipid forms. *Geochimica et Cosmochimica Acta*, 89, 102–115. <https://doi.org/10.1016/j.gca.2012.04.053>
- Liu, X.-L., Summons, R. E., & Hinrichs, K. U. (2012). Extending the known range of glycerol ether lipids in the environment: Structural assignments based on tandem mass spectral fragmentation patterns. *Rapid Communications in Mass Spectrometry*, 26(19), 2295–2302. <https://doi.org/10.1002/rcm.6355>
- Locarnini, R. A., Mishonov, A. V., Baranova, O. K., Boyer, T. P., Zweng, M. M., Garcia, H. E., et al. (2019). World Ocean Atlas 2018: Temperature. In A. Mishonov, (Eds.), *NOAA Atlas NESDIS* (Vol. 1).

- Lopes Dos Santos, R. A., Spooner, M. I., Barrows, T. T., De Deckker, P., Sinninghe Damsté, J. S., & Schouten, S. (2013). Comparison of organic (UK'37, TEXH86, LDI) and faunal proxies (foraminiferal assemblages) for reconstruction of late Quaternary sea surface temperature variability from offshore southeastern Australia. *Paleoceanography*, 28(3), 377–387. <https://doi.org/10.1002/palo.20035>
- Lü, X., Liu, X. L., Elling, F. J., Yang, H., Xie, S., Song, J., et al. (2015). Hydroxylated isoprenoid GDGTs in Chinese coastal seas and their potential as a paleotemperature proxy for mid-to-low latitude marginal seas. *Organic Geochemistry*, 89(90), 31–43. <https://doi.org/10.1016/j.orggeochem.2015.10.004>
- Mahon, K. I. (2010). The New “York” regression: Application of an improved. *Statistical Method to Geochemistry*, 38(4), 293–303. <https://doi.org/10.1080/00206819709465336>
- Martínez-Méndez, G., Hebbeln, D., Mohtadi, M., Lamy, F., De Pol-Holz, R., Reyes-Macaya, D., & Freudenthal, T. (2013). Changes in the advection of Antarctic Intermediate Water to the northern Chilean coast during the last 970 kyr. *Paleoceanography*, 28(4), 607–618. <https://doi.org/10.1002/PALO.20047>
- Massana, R., Murray, A. E., Preston, C. M., & DeLong, E. F. (1997). Vertical distribution and phylogenetic characterization of marine planktonic Archaea in the Santa Barbara Channel. *Applied and Environmental Microbiology*, 63(1), 50–56. <https://doi.org/10.1128/AEM.63.1.50-56.1997>
- Mikkonen, S., Pitkänen, M. R. A., Nieminen, T., Lipponen, A., Isokääntä, S., Arola, A., & Lehtinen, K. E. J. (2019). Technical note: Effects of uncertainties and number of data points on line fitting—a case study on new particle formation. *Atmospheric Chemistry and Physics*, 19(19), 12531–12543. <https://doi.org/10.5194/ACP-19-12531-2019>
- Mix, A. C., Tiedemann, R., Blum, P., Abrantes, F. F., Benway, H., Cacho-Lascorz, I., et al. (2003). *Proceedings of ODP, Initial Reports*, 202. College Station, TX: Ocean Drilling Program. <https://doi.org/10.2973/odp.proc.ir.202.2003>
- Mohrholz, V., Bartholomae, C. H., Van Der Plas, A. K., & Lass, H. U. (2008). The seasonal variability of the northern Benguela undercurrent and its relation to the oxygen budget on the shelf. *Continental Shelf Research*, 28(3), 424–441. <https://doi.org/10.1016/j.csr.2007.10.001>
- Mollenhauer, G., Eglinton, T. I., Hopmans, E. C., & Sinninghe Damsté, J. S. (2008). A radiocarbon-based assessment of the preservation characteristics of crenarchaeol and alkenones from continental margin sediments. *Organic Geochemistry*, 39(8), 1039–1045. <https://doi.org/10.1016/J.ORGGEOCHEM.2008.02.006>
- Mollenhauer, G., Inthorn, M., Vogt, T., Zabel, M., Sinninghe Damsté, J. S., & Eglinton, T. I. (2007). Aging of marine organic matter during cross-shelf lateral transport in the Benguela upwelling system revealed by compound-specific radiocarbon dating. *Geochemistry, Geophysics, Geosystems*, 8(9). <https://doi.org/10.1029/2007GC001603>
- Mollenhauer, G., Kienast, M., Lamy, F., Meggers, H., Schneider, R. R., Hayes, J. M., & Eglinton, T. I. (2005). An evaluation of 14C age relationships between co-occurring foraminifera, alkenones, and total organic carbon in continental margin sediments. *Paleoceanography*, 20(1), 1–12. <https://doi.org/10.1029/2004PA001103>
- Morales, C. E., Blanco, J. L., Braun, M., Reyes, H., & Silva, N. (1996). Chlorophyll- α distribution and associated oceanographic conditions in the upwelling region off northern Chile during the winter and spring 1993. *Deep-Sea Research Part I Oceanographic Research Papers*, 43(3), 267–289. [https://doi.org/10.1016/0967-0637\(96\)00015-5](https://doi.org/10.1016/0967-0637(96)00015-5)
- Moroshkin, K. V., Bunov, V. A., & Bulatov, R. P. (1970). Water circulation in the eastern South Atlantic Ocean. *Oceanology*, 10, 27–34.
- Müller, P. J., Kirst, G., Ruhland, G., Von Storch, I., & Rosell-Melé, A. (1998). Calibration of the alkenone paleotemperature index U37K based on core-tops from the eastern South Atlantic and the global ocean (60°N–60°S). *Geochimica et Cosmochimica Acta*, 62(10), 1757–1772. [https://doi.org/10.1016/S0016-7037\(98\)00097-0](https://doi.org/10.1016/S0016-7037(98)00097-0)
- Muñoz, P., Lange, C. B., Gutiérrez, D., Hebbeln, D., Salamanca, M. A., Dezileau, L., et al. (2004). Recent sedimentation and mass accumulation rates based on 210Pb along the Peru–Chile continental margin. *Deep-Sea Research Part II Topical Studies in Oceanography*, 51(20–21), 2523–2541. <https://doi.org/10.1016/j.dsr2.2004.08.015>
- Muratli, J. M., Chase, Z., McManus, J., & Mix, A. C. (2010). Ice-sheet control of continental erosion in central and southern Chile (36°–41°S) over the last 30,000 years. *Quaternary Science Reviews*, 29(23–24), 3230–3239. <https://doi.org/10.1016/j.quascirev.2010.06.037>
- Muratli, J. M., Chase, Z., Mix, A. C., & McManus, J. (2010). Increased glacial-age ventilation of the Chilean margin by Antarctic Intermediate Water. *Nature Geoscience*, 3(1), 23–26. <https://doi.org/10.1038/ngeo715>
- Ohkouchi, N., Kawamura, K., Kawahata, H., & Okada, H. (1999). Depth ranges of alkenone production in the central Pacific Ocean. *Global Biogeochemical Cycles*, 13(2), 695–704. <https://doi.org/10.1029/1998GB900024>
- Park, E., Hefter, J., Fischer, G., Hvitfeldt Iversen, M., Ramondenc, S., Nöthig, E. M., & Mollenhauer, G. (2019). Seasonality of archaeal lipid flux and GDGT-based thermometry in sinking particles of high-latitude oceans: Fram Strait (79°N) and Antarctic Polar Front (50°S). *Biogeosciences*, 16(11), 2247–2268. <https://doi.org/10.5194/bg-16-2247-2019>
- Pearson, A., McNichol, A. P., Benitez-Nelson, B. C., Hayes, J. M., & Eglinton, T. I. (2001). Origins of lipid biomarkers in Santa Monica Basin surface sediment: A case study using compound-specific $\Delta 14C$ analysis. *Geochimica et Cosmochimica Acta*, 65(18), 3123–3137. [https://doi.org/10.1016/S0016-7037\(01\)00657-3](https://doi.org/10.1016/S0016-7037(01)00657-3)
- Pelejero, C., & Grimalt, J. O. (1997). The correlation between the Uk37 index and sea surface temperatures in the warm boundary: The South China Sea. *Geochimica et Cosmochimica Acta*, 61(22), 4789–4797. [https://doi.org/10.1016/s0016-7037\(97\)00280-9](https://doi.org/10.1016/s0016-7037(97)00280-9)
- Pérez, M. E., Charles, C. D., & Berger, W. H. (2001). Late Quaternary productivity fluctuations off Angola: Evidence from benthic foraminifers, Site 1079. In G. Wefer, W. H. Berger, & C. Richte (Eds.), *Proceedings of ODP, Scientific Results*, 175 (pp. 1–19). College Station, TX: Ocean Drilling Program. <https://doi.org/10.2973/odp.proc.sr.175.213.2001>
- Pitcher, A., Villanueva, L., Hopmans, E. C., Schouten, S., Reichart, G. J., & Sinninghe Damsté, J. S. (2011). Niche segregation of ammonia-oxidizing archaea and anammox bacteria in the Arabian Sea oxygen minimum zone. *The ISME Journal*, 5(12), 1896–1904. <https://doi.org/10.1038/ISMEJ.2011.60>
- Pitcher, A., Wuchter, C., Siedenberg, K., Schouten, S., & Damsté, J. S. S. (2011). Crenarchaeol tracks winter blooms of ammonia-oxidizing Thaumarchaeota in the coastal North Sea. *Limnology & Oceanography*, 56(6), 2308–2318. <https://doi.org/10.4319/LO.2011.56.6.2308>
- Poole, R., & Tomczak, M. (1999). Optimum multiparameter analysis of the water mass structure in the Atlantic Ocean thermocline. *Deep Sea Research Part I: Oceanographic Research Papers*, 46(11), 1895–1921. [https://doi.org/10.1016/S0967-0637\(99\)00025-4](https://doi.org/10.1016/S0967-0637(99)00025-4)
- Popp, B. N., Prahl, F. G., Wallsgrove, R. J., & Tanimoto, J. (2006). Seasonal patterns of alkenone production in the subtropical oligotrophic North Pacific. *Paleoceanography*, 21(1), 1–15. <https://doi.org/10.1029/2005PA001165>
- Prahl, F. G., Popp, B. N., Karl, D. M., & Sparrow, M. A. (2005). Ecology and biogeochemistry of alkenone production at Station ALOHA. *Deep Sea Research Part I: Oceanographic Research Papers*, 52(5), 699–719. <https://doi.org/10.1016/J.DSR.2004.12.001>
- Prahl, F. G., & Wakeham, S. G. (1987). Calibration of unsaturation patterns in long-chain ketone compositions for palaeotemperature assessment. *Nature*, 330(6146), 367–369. <https://doi.org/10.1038/330367a0>
- Prokopenko, M. G., Hammond, D. E., & Stott, L. (2006). Lack of isotopic fractionation of $\delta 15N$ of organic matter during long-term diagenesis in marine sediments, ODP Leg 202, Sites 1234 and 1235. In R. Tiedemann, A. C. Mix, C. Richter, & W. F. Ruddiman (Eds.), *Proceedings of ODP, Scientific Results*, 202 (pp. 1–22). College Station, TX: Ocean Drilling Program. <https://doi.org/10.2973/odp.proc.sr.202.207.2006>

- Qin, W., Carlson, L. T., Armbrust, E. V., Devol, A. H., Moffett, J. W., Stahl, D. A., & Ingalls, A. E. (2015). Confounding effects of oxygen and temperature on the TEX86 signature of marine Thaumarchaeota. *Proceedings of the National Academy of Sciences of the United States of America*, *112*(35), 10979–10984. <https://doi.org/10.1073/pnas.1501568112>
- Rattanasriampong, R., Zhang, Y. G., Pearson, A., Hedlund, B. P., & Zhang, S. (2022). Archaeal lipids trace ecology and evolution of marine ammonia-oxidizing archaea. *Proceedings of the National Academy of Sciences of the United States of America*, *119*(31), 1–10. <https://doi.org/10.1073/pnas.2123193119>
- Regenberg, M., Regenberg, A., Garbe-Schönberg, D., Lea, D. W., Regenberg, M., Regenberg, A., et al. (2014). Global dissolution effects on planktonic foraminiferal Mg/Ca ratios controlled by the calcite-saturation state of bottom waters. *Paleoceanography*, *29*(3), 127–142. <https://doi.org/10.1002/2013PA002492>
- Reimer, P. J., Baillie, M. G. L., Bard, E., Bayliss, A., Beck, J. W., Blackwell, P. G., et al. (2009). IntCal09 and Marine09 radiocarbon age calibration curves, 0–50,000 years cal BP. *Radiocarbon*, *51*(4), 1111–1150. <https://doi.org/10.1017/S003822200034202>
- Rühlemann, C., Mulitza, S., Lohmann, G., Paul, A., Prange, M., & Wefer, G. (2004). Intermediate depth warming in the tropical Atlantic related to weakened thermohaline circulation: Combining paleoclimate data and modeling results for the last deglaciation. *Paleoceanography*, *19*(1), 1–10. <https://doi.org/10.1029/2003PA000948>
- Schouten, S., Forster, A., Panoto, F. E., & Sinninghe Damsté, J. S. (2007). Towards calibration of the TEX86 palaeothermometer for tropical sea surface temperatures in ancient greenhouse worlds. *Organic Geochemistry*, *38*(9), 1537–1546. <https://doi.org/10.1016/j.orggeochem.2007.05.014>
- Schouten, S., Hopmans, E. C., Baas, M., Boumann, H., Standfest, S., Könneke, M., et al. (2008). Intact membrane lipids of “Candidatus Nitrosopumilus maritimus,” a cultivated representative of the cosmopolitan mesophilic group I crenarchaeota. *Applied and Environmental Microbiology*, *74*(8), 2433–2440. <https://doi.org/10.1128/AEM.01709-07/ASSET/60849007-EC9E-4539-A0D1-AA6B837D4DE8/ASSETS/GRAPHIC/ZAM0080887670005>
- Schouten, S., Hopmans, E. C., Schefuß, E., & Sinninghe Damsté, J. S. (2002). Distributional variations in marine crenarchaeotal membrane lipids: A new tool for reconstructing ancient sea water temperatures? *Earth and Planetary Science Letters*, *204*(1–2), 265–274. [https://doi.org/10.1016/S0012-821X\(02\)00979-2](https://doi.org/10.1016/S0012-821X(02)00979-2)
- Schouten, S., Pitcher, A., Hopmans, E. C., Villanueva, L., van Bleijswijk, J., & Sinninghe Damsté, J. S. (2012). Intact polar and core glycerol dibiphytanyl glycerol tetraether lipids in the Arabian Sea oxygen minimum zone: I. Selective preservation and degradation in the water column and consequences for the TEX86. *Geochimica et Cosmochimica Acta*, *98*, 228–243. <https://doi.org/10.1016/j.gca.2012.05.002>
- Shah, S. R., Mollenhauer, G., Ohkouchi, N., Eglinton, T. I., & Pearson, A. (2008). Origins of archaeal tetraether lipids in sediments: Insights from radiocarbon analysis. *Geochimica et Cosmochimica Acta*, *72*(18), 4577–4594. <https://doi.org/10.1016/j.gca.2008.06.021>
- Shannon, L. V., Agenbag, J. J., & L Buys, M. E. (1987). Large- and mesoscale features of the Angola-Benguela front. *South African Journal of Marine Science*, *5*(1), 11–34. <https://doi.org/10.2989/025776187784522261>
- Shannon, L. V., & Nelson, G. (1996). The Benguela: Large scale features and processes and system variability. *The South Atlantic*, 163–210. https://doi.org/10.1007/978-3-642-80353-6_9
- Siegfried, L., Schmidt, M., Mohrholz, V., Pogrzeba, H., Nardini, P., Bö Ttinger, M., & Scheuermann, G. (2019). The tropical-subtropical coupling in the Southeast Atlantic from the perspective of the northern Benguela upwelling system. <https://doi.org/10.1371/journal.pone.0210083>
- Sinninghe Damsté, J. S., Rijpstra, W. I. C., Hopmans, E. C., Jung, M. Y., Kim, J. G., Rhee, S. K., et al. (2012). Intact polar and core glycerol dibiphytanyl glycerol tetraether lipids of group I.1a and I.1b Thaumarchaeota in soil. *Applied and Environmental Microbiology*, *78*(19), 6866–6874. <https://doi.org/10.1128/AEM.01681-12>
- Sinninghe Damsté, J. S., Rijpstra, W. I. C., & Reichart, G.-J. (2002a). The influence of oxic degradation on the sedimentary biomarker record II. Evidence from Arabian Sea sediments. *Geochimica et Cosmochimica Acta*, *66*(15), 2737–2754. [https://doi.org/10.1016/S0016-7037\(02\)00865-7](https://doi.org/10.1016/S0016-7037(02)00865-7)
- Sinninghe Damsté, J. S., Schouten, S., Hopmans, E. C., Van Duin, A. C. T., & Geenevasen, J. A. J. (2002b). Crenarchaeol: The characteristic core glycerol dibiphytanyl glycerol tetraether membrane lipid of cosmopolitan pelagic crenarchaeota. *Journal of Lipid Research*, *43*(10), 1641–1651. <https://doi.org/10.1194/jlr.M200148-JLR200>
- Sinninghe Damsté, J. S., Weber, Y., Zopfi, J., Lehmann, M. F., & Niemann, H. (2022). Distributions and sources of isoprenoidal GDGTs in Lake Lugano and other central European (peri-)alpine lakes: Lessons for their use as paleotemperature proxies. *Quaternary Science Reviews*, *277*, 107352. <https://doi.org/10.1016/j.quascirev.2021.107352>
- Sluijs, A., Frieling, J. N., Inglis, G., Nierop, K. G. J., Peterse, F., Sangiorgi, F., & Schouten, S. (2020). Late Paleocene-early Eocene Arctic Ocean sea surface temperatures: Reassessing biomarker paleothermometry at Lomonosov Ridge. *Climate of the Past*, *16*(6), 2381–2400. <https://doi.org/10.5194/cp-16-2381-2020>
- Sluijs, A., Schouten, S., Pagani, M., Woltering, M., Brinkhuis, H., Damsté, J. S. S., et al. (2006). Subtropical Arctic Ocean temperatures during the Palaeocene/Eocene thermal maximum. *Nature*, *441*(7093), 610–613. <https://doi.org/10.1038/NATURE04668>
- Sollai, M., Hopmans, E. C., Schouten, S., Keil, R. G., & Sinninghe Damsté, J. S. (2015). Intact polar lipids of Thaumarchaeota and anammox bacteria as indicators of N cycling in the eastern tropical North Pacific oxygen-deficient zone. *Biogeosciences*, *12*(15), 4725–4737. <https://doi.org/10.5194/bg-12-4725-2015>
- Sollai, M., Villanueva, L., Hopmans, E. C., Keil, R. G., & Damsté, J. S. S. (2019). Archaeal sources of intact membrane lipid biomarkers in the oxygen deficient zone of the eastern tropical South Pacific. *Frontiers in Microbiology*, *10*(APR). <https://doi.org/10.3389/FMICB.2019.00765/PDF>
- Spencer-Jones, C. L., McClymont, E. L., Bale, N. J., Hopmans, E. C., Schouten, S., Müller, J., et al. (2021). Archaeal intact polar lipids in polar waters: A comparison between the Amundsen and Scotia seas. *Biogeosciences*, *18*(11), 3485–3504. <https://doi.org/10.5194/bg-18-3485-2021>
- Steinig, S., Dummann, W., Park, W., Latif, M., Kusch, S., Hofmann, P., & Flögel, S. (2020). Evidence for a regional warm bias in the Early Cretaceous TEX86 record. *Earth and Planetary Science Letters*, *539*, 116184. <https://doi.org/10.1016/j.epsl.2020.116184>
- Strub, P. T., Mesías, M. J., Montecino, V., Rutllant, J., & Salinas, S. (1998). Coastal ocean circulation off Western South America coastal segment. *The Sea*.
- Summons, R. E., Embaye, T., Jahnke, L. L., & Baumgartner, M. (2002). Molecular signatures of methanogens in cultures and environmental samples. Retrieved from https://www.researchgate.net/publication/253369862_Molecular_Signatures_of_Methanogens_in_Cultures_and_Environmental_Samples
- Taylor, K. W. R., Huber, M., Hollis, C. J., Hernandez-Sanchez, M. T., & Pancost, R. D. (2013). Re-evaluating modern and Palaeogene GDGT distributions: Implications for SST reconstructions. *Global and Planetary Change*, *108*, 158–174. <https://doi.org/10.1016/j.gloplacha.2013.06.011>
- Techtman, S. M., Mahmoudi, N., Whitt, K. T., Campa, M. F., Fortney, J. L., Joyner, D. C., & Hazen, T. C. (2017). Comparison of Thaumarchaeotal populations from four deep sea basins. *FEMS Microbiology Ecology*, *93*(11). <https://doi.org/10.1093/FEMSEC/FIX128>
- Ternois, Y., Sicre, M. A., Boireau, A., Marty, J. C., & Miquel, J. C. (1996). Production pattern of alkenones in the Mediterranean Sea. *Geophysical Research Letters*, *23*(22), 3171–3174. <https://doi.org/10.1029/96GL02910>

- Thiel, M., Macaya, E., Acuña, E., Arntz, W., Bastias, H., Brokordt, K., et al. (2007). The Humboldt current system of Northern and Central Chile. <https://doi.org/10.1201/9781420050943.ch6>
- Tiedemann, R., & Mix, A. (2007). Leg 202 synthesis: Southeast Pacific paleoceanography. In R. Tiedemann, A. C. Mix, C. Richter, & W. F. Ruddiman (Eds.), *Proceedings of ODP, Scientific Results, 202* (pp. 1–56). College Station, TX: Ocean Drilling Program. <https://doi.org/10.2973/odp.proc.sr.202.201.2007>
- Tierney, J. E. (2013). Biomarker-based Inferences of past climate: The TEX86 paleotemperature proxy. In *Treatise on geochemistry* (2nd ed., Vol. 12). Elsevier Ltd. <https://doi.org/10.1016/B978-0-08-095975-7.01032-9>
- Tierney, J. E., & Tingley, M. P. (2014). A Bayesian, spatially-varying calibration model for the TEX86 proxy. *Geochimica et Cosmochimica Acta*, 127, 83–106. <https://doi.org/10.1016/j.gca.2013.11.026>
- Tierney, J. E., & Tingley, M. P. (2015). A TEX 86 surface sediment database and extended Bayesian calibration. *Scientific Data*, 2, 1–10. <https://doi.org/10.1038/sdata.2015.29>
- Varma, D., Hattig, K., van der Meer Marcel, T. J., Reichart, G.-J., & Schouten, S. (2023). SST Proxies Chilean (ODP Leg 202 site 1235 and site 1234) and Angola Margin (ODP Leg 175 site 1078 and site 1079). [Dataset]. PANGAEA. <https://doi.org/10.1594/PANGAEA.957090>
- Villanueva, L., Schouten, S., Damsté, J. S. S., & Box, P. O. (2015). Depth-related distribution of a key gene of the tetraether lipid biosynthetic pathway in marine Thaumarchaeota. *Environmental Microbiology*, 17(10), 3527–3539. <https://doi.org/10.1111/1462-2920.12508>
- Vorrath, M. E., Müller, J., Rebolledo, L., Cárdenas, P., Shi, X., Esper, O., et al. (2020). Sea ice dynamics in the Bransfield strait, Antarctic Peninsula, during the past 240 years: A multi-proxy intercomparison study. *Climate of the Past*, 16(6), 2459–2483. <https://doi.org/10.5194/CP-16-2459-2020>
- Wainer, I., Goes, M., Murphy, L. N., & Brady, E. (2012). Changes in the intermediate water mass formation rates in the global ocean for the Last Glacial Maximum, mid-Holocene and pre-industrial climates. *Paleoceanography*, 27(3). <https://doi.org/10.1029/2012PA002290>
- Wakeham, S. G., Lewis, C. M., Hopmans, E. C., Schouten, S., & Sinninghe Damsté, J. S. (2003). Archaea mediate anaerobic oxidation of methane in deep euxinic waters of the Black Sea. *Geochimica et Cosmochimica Acta*, 67(7), 1359–1374. [https://doi.org/10.1016/S0016-7037\(02\)01220-6](https://doi.org/10.1016/S0016-7037(02)01220-6)
- Wang, Y., Li, D. W., Sachs, J. P., Hu, J., Cao, Y., Li, L., et al. (2019). Vertical distribution of isoprenoid GDGTs in suspended particles from the East China Sea shelf and implications for sedimentary TEX86H records. *Organic Geochemistry*, 136, 103895. <https://doi.org/10.1016/j.orggeochem.2019.07.004>
- Wefer, G., Berger, W. H., Richter, C., & Shipboard Scientific Party. (1998). *Proceedings of ODP, Initial Reports, 175*. College Station, TX: Ocean Drilling Program. <https://doi.org/10.2973/odp.proc.ir.175.1998>
- Weijers, J. W. H., Schouten, S., Spaargaren, O. C., & Sinninghe Damsté, J. S. (2006). Occurrence and distribution of tetraether membrane lipids in soils: Implications for the use of the TEX86 proxy and the BIT index. *Organic Geochemistry*, 37(12), 1680–1693. <https://doi.org/10.1016/J.ORGEOCHEM.2006.07.018>
- Wolhowe, M. D., Prahl, F. G., White, A. E., Popp, B. N., & Rosas-Navarro, A. (2014). A biomarker perspective on coccolithophorid growth and export in a stratified sea. *Progress in Oceanography*, 122, 65–76. <https://doi.org/10.1016/j.pcean.2013.12.001>
- Wuchter, C., Schouten, S., Coolen, M. J. L., & Sinninghe Damsté, J. S. (2004). Temperature-dependent variation in the distribution of tetraether membrane lipids of marine Crenarchaeota: Implications for TEX86 paleothermometry. *Paleoceanography*, 19(4), 1–10. <https://doi.org/10.1029/2004PA001041>
- Wuchter, C., Schouten, S., Wakeham, S. G., & Sinninghe Damsté, J. S. (2005). Temporal and spatial variation in tetraether membrane lipids of marine Crenarchaeota in particulate organic matter: Implications for TEX86 paleothermometry. *Paleoceanography*, 20(3), 1–11. <https://doi.org/10.1029/2004PA001110>
- Yang, Y., Gao, C., Dang, X., Ruan, X., Lü, X., Xie, S., et al. (2018). Assessing hydroxylated isoprenoid GDGTs as a paleothermometer for the tropical South China Sea. *Organic Geochemistry*, 115, 156–165. <https://doi.org/10.1016/j.orggeochem.2017.10.014>
- York, D., Evensen, N. M., Martínez, M. L., & De Basabe Delgado, J. (2004). Unified equations for the slope, intercept, and standard errors of the best straight line. *American Journal of Physics*, 72(3), 367–375. <https://doi.org/10.1119/1.1632486>
- Zeng, Z., Liu, X.-L., Farley, K. R., Wei, J. H., Metcalf, W. W., Summons, R. E., & Welander, P. V. (2019). GDGT cyclization proteins identify the dominant archaeal sources of tetraether lipids in the ocean. *Proceedings of the National Academy of Sciences of the United States of America*, 116(45), 22505–22511. <https://doi.org/10.1073/pnas.1909306116>
- Zhang, Y. G., & Liu, X. (2018). Export depth of the TEX86 signal. *Paleoceanography and Paleoclimatology*, 33(7), 666–671. <https://doi.org/10.1029/2018PA003337>

References From the Supporting Information

- Andersen, K. K., Azuma, N., Barnola, J. M., Bigler, M., Biscaye, P., Caillon, N., et al. (2004). High-resolution record of Northern Hemisphere climate extending into the last interglacial period. *Nature*, 431(7005), 147–151. <https://doi.org/10.1038/NATURE02805>
- Jouzel, J., Masson-Delmotte, V., Cattani, O., Dreyfus, G., Falourd, S., Hoffmann, G., et al. (2007). Orbital and millennial Antarctic climate variability over the past 800,000 years. *Science*, 317(5839), 793–796. https://doi.org/10.1126/SCIENCE.1141038/SUPPL_FILE/JOUZEL